Reliability Based Topology Optimization of a Linear Piezoelectric Micromotor Using the Cell-Based Smoothed Finite Element Method

Mohsen Sadeghbeigi Olyaie[1]**, Mohammad Reza Razfar**[2]
Edward J. Kansa[3]

Abstract: This paper presents integration of reliability analysis with topology optimization design for a linear mircroactuator, including multitude cantilever piezoelectric bimorphs. Each microbimoph in the mechanism can be actuated in both axial and flexural modes simultaneously. We consider quasi-static and linear conditions, and the smoothed finite element method (S-FEM) is employed in the analysis of piezoelectric effects. Since microfabrication methods are used for manufacturing this type of actuator, uncertainty variables become very important. Hence, these variables are considered as constraints during our topology optimization design process and reliability based topology optimization (RBTO) is conducted. To avoid the overly-stiff behavior in FEM modeling, a relatively new numerical method known as the cell-based smoothed finite element method (CS-FEM, as a branch of S-FEM) has been introduced first time for our RBTO problem. Reliability analysis has been conducted using performance measure approach (PMA), advanced mean value (AMV) and first order reliability method (FORM). After finding random design points, topology optimization procedure is implemented using a solid isotropic material with a penalization (SIMP) and method of moving asymptotes (MMA) optimizer. Numerical tests show that the accuracy and efficiency of numerical results using softer CS-FEM in RBTO problems are substantially improved compared to the FEM.

Keywords: RBTO, Topology Optimization, Smoothed Finite Element Method, Micromotor, Piezoelectric

---

[1] Department of Mechanical Engineering, Amirkabir University of Technology, Tehran, Iran, Email: m.sadeghbeigi@aut.ac.ir

[2] Corresponding author, Department of Mechanical Engineering, Amirkabir University of Technology, Tehran, Iran, Email: razfar@aut.ac.ir

[3] Department of Mechanical and Aeronautical Engineering, University of California-Davis, Davis, CA 95616, USA, Email: ejkansa@ucdavis.edu

1 Introduction

Because of various advanced applications of actuators in industry, the dimensions of linear actuators are gradually being reduced to beyond the size of microelectromechanical systems (MEMS). Among actuation mechanisms, piezoelectric microactuators have been found to be superior in providing actuation forces, see Ueha and Tomikawa (1993). Making use of the piezoelectric effect was first discovered by the Curie brothers in 1880, in which both direct (sensing) and inverse (actuation) effects were identified, see Yang (2006).

Determining the optimum design of piezoelectric structures requires a systematic approach to reduce the dimensions of these materials to make them more efficient, see Frecker (2003); Irschik (2002). Typically, there are two strategies for optimizing the design of structures: deterministic and reliability based optimizations, see Frangopol (1995). A deterministic optimization technique determines the optimum solution using fixed design parameters, whereas a reliability-based optimization considers variations of design parameters. Since device fabrication processes are usually accompanied with some inaccuracies, the existence of significant uncertainties in material properties or the geometry of these structures are often probable. This issue becomes even more critical for small-sized structures, see Stark (1999); Tbata and Tsuchiya (2007).

Topology optimization is a branch of optimization methods for finding optimal material distributions in a given design domain, see Bendsoe and Sigmund (2003). The origin of the topology optimization concept goes back to 1904, at which time Michell minimized the weight of a structure under stress constraints, see Spillers and MacBain (2009). However, the rapid development in topology optimization field started after the landmark paper of Bendsoe and Kikuchi in 1988. Similar to other optimization techniques, this method can be divided into deterministic topology optimization (DTO) and reliability based topology optimization (RBTO). There are two approaches for RBTO analyses: the independent method and the nested method; because of the low computational cost of the independent method, it was chosen for use in this research, see Kharmanda, Olhoff and El-Hami (2004); Kharmanda, Olhoff, Mohamed and Lemaire (2004). Based on this approach, reliability design variables should be computed first through a reliability evaluation model, and the optimization process is then performed by using these design points as input data. The reliability based optimization procedure is briefly explained in figure 1.

Reliability evaluations in RBTO can be implemented using techniques such as the Monte Carlo simulation (MCS), see Buslenko, Golenko, Shreider, Sobol and Sragowich (1964), or approximation methods such as the reliability index approach

(RIA) or performance measure approach (PMA), see Jae-Ohk, Young-Soon and Wom-Sun (2002); Youn, Choi and Park (2003). Because MCS usually requires a large number of evaluations for objective functions related to uncertainties amounts, RIA or PMA are more frequently used, see Youn, Choi and Park (2003). In addition, for a system with small nonlinearity, the first order reliability method (FORM) can accelerate reliability computations, see Bae, Wang and Choi (2002); Allen, Raulli, Maute and Frangopol (2004); Raulli and Maute (2009). For a convex set, the use of PMA in conjunction with the advanced mean value (AMV) optimizer is usually a better candidate; see Youn, Choi and Park (2003).

To date, however, topology optimization using a solid isotropic material with a penalization (SIMP) approximation is the simplest and most popular technique; see Rozvany, Zhou and Birker (1992). This technique penalizes the intermediate density of each element, as a design variable, to an analogue value using power law approximations, see Bendsoe (1989). Design variables in the optimization process can also be updated through algorithms such as sequence linear programming (SLP) or sequence quadratic programming (SQP), see Nocedal and Wrigh (2006). For example, Svanberg (1987) proposed a powerful optimizer tool known as the method of moving asymptotes (MMA) for this purpose.

As can be observed from figure 1, the major time-consuming task under the updating loop and reliability evaluation needs to be handled by a stable and efficient numerical method such as the finite element method (FEM). For piezoelectric analyses, due to the overly stiff behavior of the FEM obtained from the overestimation of the stiffness matrix, numerical results usually have low stress accuracy and the solution is sensitive to element distortions, see Benjeddou (2000); Allik and Hughes (1970). To overcome these drawbacks, finite element methods such as the piezoelectric finite element with drilling degrees of freedom, see Long, Loveday and Groenwold (2006), hybrid formulations, see Sze, Yang and Yao (2004), and meshless methods such as the meshless point collocation method (PCM) and radial point interpolation methods (RPIM), see Ohs and Aluru (2001); Liu, Dai, Lim and Gu (2003), have been developed.

A method that combines parts of the standard FEM and meshless techniques, see Chen, Wu and Yoon (2001), called the smoothed finite element method (S-FEM), was developed by Liu, Dai and Nguyen in 2007. This method states that numerical analyses of static and dynamic problems through S-FEMs are always more stable than standard FEMs, due to softening effects provided by smoothing operations in the S-FEM, see Bordas, Rabczuk, Hung, Nguyen, Natarajan, Bog, Quan and Hiep (2010). As such, the S-FEM numerical results are often found to be even more accurate than those of standard FEMs with the same degrees of freedom, see Liu, Nguyen and Lam (2009); Liu and Nguyen (2010); Liu, Nguyen, Dai and Lam
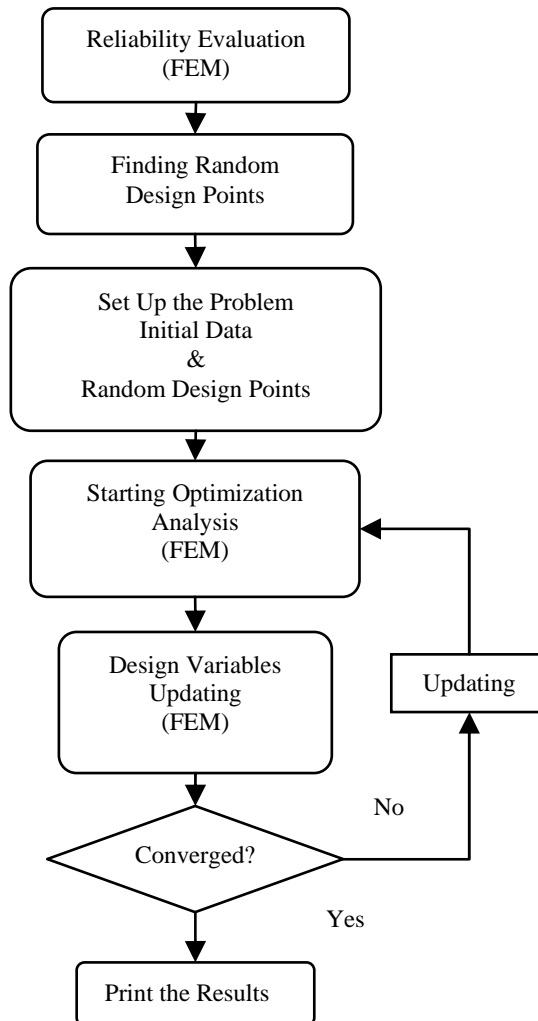
Figure 1: Typical flowchart for a numerical reliability based optimization.

(2007); Liu, Nguyen X.H. and Nguyen T.T. (2010).

Static and eigenvalue models of piezoelectric structures using an edge-based S-FEM were then developed by Nguyen X.H., Liu, Nguyen T.T. and Nguyen C.T. in 2009. Their results showed good agreement with analytical solutions, and also had more accuracy than standard FEMs. To date, most investigations on piezoelectric topology optimization, such as that by Silva and Kikuchi (1999); Silva (2003); Begg and Liu (2000); Carbonari, Nader and Silva (2006); Carbonari, Silva and Nishiwaki (2005); Kogl and Silva (2005); Kang and Wang (2010); Donoso and Sigmund (2009); Kim J.E., Kim D.S., Ma and Kim Y.Y. (2010), have focused on deterministic topology optimization through standard FEM algorithms. Because of the important role of reliability for MEMS sized-structures, the RBTO of the considered piezoelectric micromotor proposed by Friend, Umeshima, Ishii, Nakamura and Ueha in 2004, using the softer CS-FEM will be further discussed in this paper.

The remainder of this paper is organized as follows. The design concept of an actuator will be discussed in section 2. The S-FEM and cell-based S-FEM are then introduced in section 3. The framework of topology optimization and RBTO analysis will be explained in section 4. In section 5, the problem algorithm will be explained. In section6, the DTO and RBTO numerical results of this micromotor based on Q4-FEM, T3-FEM and CS-FEM will be compared, examined and discussed in detail. Finally, conclusions of this research will be briefly discussed.

2   Concept design of the used piezoelectric linear micromotor

Recently, linear actuators have been used in various engineering applications for fields such as aerospace, robotics, optics, and medical science. Because these actuators need to fit into small devices such as cell phones, microrobotics, and those used in microsurgeries, they are moving toward and beyond MEMS size.

Many smart materials such as shape memory alloys, magnetostrictives, electrostrictives, and piezoelectric materials can be used for actuation in these systems, see Moskalik and Brei (1999). However, shape memory alloys usually have slow dynamic responses, electro- or magnetostrictives have nonlinear responses, and piezoelectric materials produce limit strains, see Moskalik and Brei (1999). Because of the rapid dynamic responses, large actuation force, and fairly linear behavior of piezoelectric materials, these materials are the preferred choices for various purposes, including actuation and vibration controls, see Irschik (2002). To overcome limitations in displacement generation, different actuation architectures have been developed, see Moskalik and Brei (1999), including: 1) internally leveraged amplifiers such as bimorph cantilevers, and 2) externally leveraged mechanisms such as the X-frame and Moonie. The bimorph cantilever has been found to be capable of

producing larger deflections than other configurations, see Wang, Zhang, Xu, Liu and Cross (1999).

The design concept of the linear micromotor used in this study is based on the axial and transverse motions of bimorph piezoelectric cantilevers, see Friend, Umeshima, Ishii, Nakamura and Ueha (2004). Figure 2 schematically shows the layout of these cantilever bimorphs and the operating mechanism of this linear motor. Detailed information about each bimorph can be seen in figure 3; in the figure, each beam includes an elastic material interface with low magnetic permeability (such as phosphor bronze), two piezoelectric layers with the same polarization direction, and finally some relevant electrodes for applying electric fields. The initial state of the piezoelectric beam is shown in figure 4(a). By applying an electric voltage on electrodes 2 and 4 (figure 4(b)), an axial displacement will be produced; by just applying a voltage on electrodes 1 and 3 a transverse movement is achievable (figure 4(c)). Finally, by applying an electric field simultaneously on all four electrodes, an elliptical motion will be generated (figure 4(d)). By creating a suitable phase shifting on the piezoelectric sequentially bimorphs, and then by generating a preload force on the system, a linear motion will be produced (figure 2). Recently, a Swedish company (PiezoMotor AB) has been commercially manufacturing this type of linear motor.

3 Cell-based smoothed finite element method formulations for piezoelectric problems

Based on the variational formulation for a two-dimensional piezoelectric structure, the energy functional (L) for the design domain (Ω) can be expressed as, see Benjeddou (2000); Allik and Hughes (1970); Nguyen X.H., Liu, Nguyen T.T. and Nguyen C.T. (2009):

$$L = \int_{\Omega} \left[\frac{1}{2}\rho \dot{\mathbf{U}}^{\mathrm{T}}\mathbf{U} - \frac{1}{2}\mathbf{S}^{\mathrm{T}}\mathbf{T} + \frac{1}{2}\mathbf{D}^{\mathrm{T}}\mathbf{E} + \mathbf{U}^{\mathrm{T}}\mathbf{F}_{\mathrm{S}} - \varphi\mathbf{Q}_{\mathrm{S}} \right] d\Omega + \sum \mathbf{U}^{\mathrm{T}}\mathbf{F}_{\mathrm{P}} - \sum \varphi\mathbf{Q}_{\mathrm{P}} \quad (1)$$

where $\mathbf{U}$ and $\dot{\mathbf{U}}$ are the mechanical displacement and velocity, respectively, φ relates to the electric potential vector, $\mathbf{T}$ and $\mathbf{S}$ denote the stress and strain vectors, and $\mathbf{D}$ and $\mathbf{E}$ are the electric displacement and electric field vectors. In addition, $\mathbf{F}_{\mathrm{S}}$ and $\mathbf{F}_{\mathrm{P}}$ express the surface and point loads on the design domain, and $\mathbf{Q}_{\mathrm{S}}$, $\mathbf{Q}_{\mathrm{P}}$, and ρ are the surface and point electric charge loads and the density.

For linear conditions, the matrix form of the constitutive equation for a piezoelectric structure can be written as:

$$\begin{Bmatrix} \mathbf{T} \\ \mathbf{D} \end{Bmatrix} = \begin{bmatrix} c_E & -e^{\mathrm{T}} \\ e & \varepsilon_s \end{bmatrix} \begin{Bmatrix} \mathbf{S} \\ \mathbf{E} \end{Bmatrix}. \quad (2)$$

In this equation, c_E, e, and ε_s are the elastic material property matrix at a constant electric field, and piezoelectric and dielectric matrices at a constant mechanical strain, respectively. For a standard FEM analysis, the compatibility relations between the strain-displacement and electric field-potential have the forms:

$$\mathbf{S} = \nabla \mathbf{U} \tag{3}$$

$$\mathbf{E} = -grad(\varphi) \tag{4}$$

$$\nabla = \begin{bmatrix} \frac{\partial}{\partial x} & 0 & \frac{\partial}{\partial y} \\ 0 & \frac{\partial}{\partial y} & \frac{\partial}{\partial x} \end{bmatrix}. \tag{5}$$
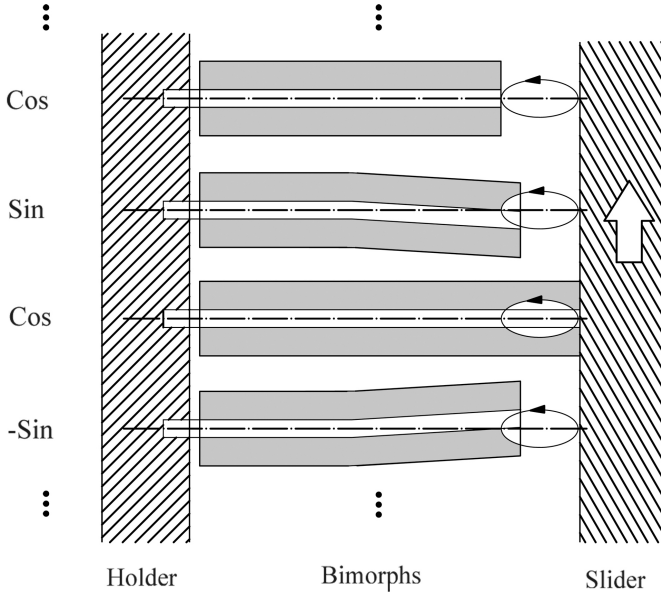
Figure 2: Operational mechanism of the considered piezoelectric linear micromotor, see Friend, Umeshima, Ishii, Nakamura and Ueha (2004).

When using a standard FEM, the unknown displacement and electric potential can be approximated as:

$$\mathbf{U}(x) = \sum_{I=1}^{n} \begin{bmatrix} \mathbf{N}_I(x) & 0 \\ 0 & \mathbf{N}_I(x) \end{bmatrix} \mathbf{U}_I; \quad \varphi(x) = \sum_{I=1}^{n} \mathbf{N}_I(x) \varphi_I \tag{6}$$
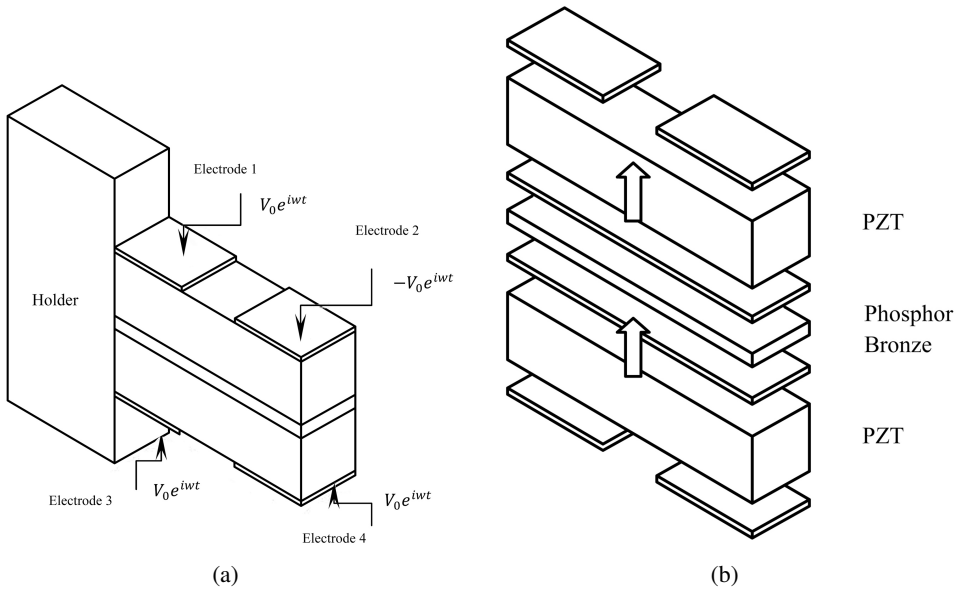
Figure 3: Bimorph beam used to construct the linear micromotor: (a) assembled and (b) its components; see Friend, Umeshima, Ishii, Nakamura and Ueha (2004).

where n, $\mathbf{U}_I$, φ_I, and $\mathbf{N}_I(x)$ are the total number of nodes in the design domain, nodal displacement vector, nodal electric potential vector, and (linear) shape function, respectively. Substitution of Eq. (6) into eqs. (3) and (4) leads to:

$$\mathbf{S} = \nabla \mathbf{U} = \sum_{I=1}^{n} \mathbf{B}_{UI} \mathbf{U}_I \tag{7}$$

$$\mathbf{E} = -grad(\varphi) = \sum_{I=1}^{n} \mathbf{B}_{\varphi I} \varphi_I \tag{8}$$

in which:

$$\mathbf{B}_{UI} = \begin{bmatrix} \mathbf{N}_{I,x} & 0 \\ 0 & \mathbf{N}_{I,y} \\ \mathbf{N}_{I,y} & \mathbf{N}_{I,x} \end{bmatrix}$$

and

$$\mathbf{B}_{\varphi I} = \begin{bmatrix} \mathbf{N}_{I,x} \\ \mathbf{N}_{I,y} \end{bmatrix}. \tag{9}$$
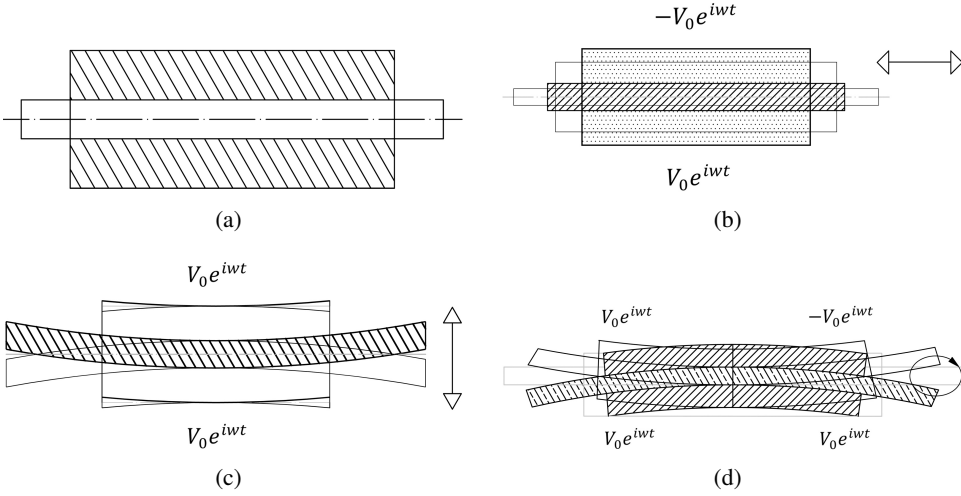
Figure 4: Vibration modes for a free-free piezoelectric bimorph: (a) initial state, (b) axial motion, (c) transverse motion, and (d) elliptical motion, see Friend, Umeshima, Ishii, Nakamura and Ueha (2004).

Then, based on Hamilton's principle, we require:

$$\delta \int_{t_1}^{t_2} L \mathrm{d}t = 0 \qquad (10)$$

where t is the time. Substituting Eqs. (6) to (8) into Eq. (10), the general linear discretized standard FEM form of piezoelectric structures having a damping consideration ($\mathbf{C}$) can be derived as, see Jensen (2009):

$$\mathbf{M}\ddot{\mathbf{d}} + \mathbf{C}\dot{\mathbf{d}} + \mathbf{K}\mathbf{d} = \mathbf{P}(t). \qquad (11)$$

Note that the definitions of the displacement vector ($\mathbf{d}$), mass matrix ($\mathbf{M}$), stiffness matrix ($\mathbf{K}$), and loading vector ($\mathbf{P}(t)$) in Eq. (11) are:

$$\mathbf{d} = \left\{ \begin{matrix} \mathbf{U} \\ \varphi \end{matrix} \right\} \qquad (12)$$

$$\mathbf{M} = \begin{bmatrix} m & 0 \\ 0 & 0 \end{bmatrix} \qquad (13)$$

$$\mathbf{K} = \begin{bmatrix} \mathbf{k}_{uu} & \mathbf{k}_{u\varphi} \\ \mathbf{k}_{u\varphi} & \mathbf{k}_{\varphi\varphi} \end{bmatrix} \qquad (14)$$

$$\mathbf{P} = \begin{Bmatrix} \mathbf{F} \\ \mathbf{Q} \end{Bmatrix}. \tag{15}$$

Then, for the plane stress or plane strain conditions:

$$\mathbf{m} = \int_{\Omega} \rho \mathbf{N}_u^{\mathrm{T}} \mathbf{N}_u \mathrm{d}\Omega \tag{16}$$

$$\mathbf{k}_{uu} = \int_{\Omega} \mathbf{B}_u^{\mathrm{T}} c_E \mathbf{B}_u \mathrm{d}\Omega \tag{17}$$

$$\mathbf{k}_{u\varphi} = \int_{\Omega} \mathbf{B}_u^{\mathrm{T}} e^{\mathrm{T}} \mathbf{B}_\varphi \mathrm{d}\Omega \tag{18}$$

$$\mathbf{k}_{\varphi\varphi} = -\int_{\Omega} \mathbf{B}_u^{\mathrm{T}} \varepsilon_s \mathbf{B}_\varphi \mathrm{d}\Omega \tag{19}$$

$$\mathbf{F} = \int_{\Omega} \mathbf{N}_u^{\mathrm{T}} \mathbf{F}_s \mathrm{d}\Omega + \mathbf{N}_u^{\mathrm{T}} \mathbf{F}_{\mathrm{P}} \tag{20}$$

$$\mathbf{Q} = -\int_{\Omega} \mathbf{N}_\varphi^{\mathrm{T}} \mathbf{Q}_s \mathrm{d}\Omega - \mathbf{N}_\varphi^{\mathrm{T}} \mathbf{Q}_{\mathrm{p}}. \tag{21}$$

If a proportional damping (Rayleigh) matrix has been considered, then:

$$\mathbf{C}(\rho) = \alpha \mathbf{M} + \vartheta \mathbf{K} \tag{22}$$

where α and ϑ are the constant prescribed damping coefficients. For a complex form, Eq. (11) can be changed to:

$$\mathbf{M}(\rho)\ddot{\hat{d}} + \mathbf{C}(\rho)\dot{\hat{d}} + \mathbf{K}(\rho)\hat{d} = \hat{\mathbf{P}}(\rho, t). \tag{23}$$

In this equation, $\hat{d}$ and $\hat{\mathbf{P}}(\rho, t)$ are the transformed shapes of instantaneous displacement and load vectors, respectively. For topology optimization applications, it should be considered that all the design parameters in Eq. (23) are collected in the density of each element (ρ) as the design variable.

When the S-FEM is used, the problem domain is also discretized using the same elements as in the standard FEM, through a set of smoothing domains is created on top of the element mesh. The (compatible) strains given in Eq. (3) are then smoothed over each of the smoothing domains.

Based on the type of smoothing domain used, there are five possible S-FEM versions, see Liu and Nguyen (2010); Liu, Nguyen X.H. and Nguyen T.T. (2010):

1) cell-based S-FEM (CS-FEM), 2) node-based S-FEM (NS-FEM), 3) edge-based S-FEM (ES-FEM), 4) face-based S-FEM (FS-FEM), and 5) alpha-FEM.

The main difference between these versions is the type of smoothing domain used for strain smoothing. For example, in the ES-FEM the smoothing domains are constructed based on the edge of each standard triangular element; for NS-FEM, the smoothing domains are created according to the nodes and middle edge points of each element. The choice of the method generally depends on the requirement on the solution properties. For this study, because of the multi-material and multi-layer conditions CS-FEM is preferred.

For CS-FEM, the smoothing domains are constructed based on the cells located inside each element. These domains are linearly independent such that $\Omega = \cup_{c=1}^{n_c} \Omega^{(c)}$ and for each $i \neq j$, $\Omega^{(i)} \cap \Omega^{(j)} = \emptyset$. Here, Ω is the total design domain, $\Omega^{(i \ or \ j)}$ is the domain of $(i \ or \ j)^{th}$ smoothing domain, and n_c is the total number of cells inside the design domain. Figure 5 schematically presents the smoothing domains associated with the different number of cells (c) for a quadrilateral CS-FEM, see Liu, Nguyen X.H. and Nguyen T.T. (2010).
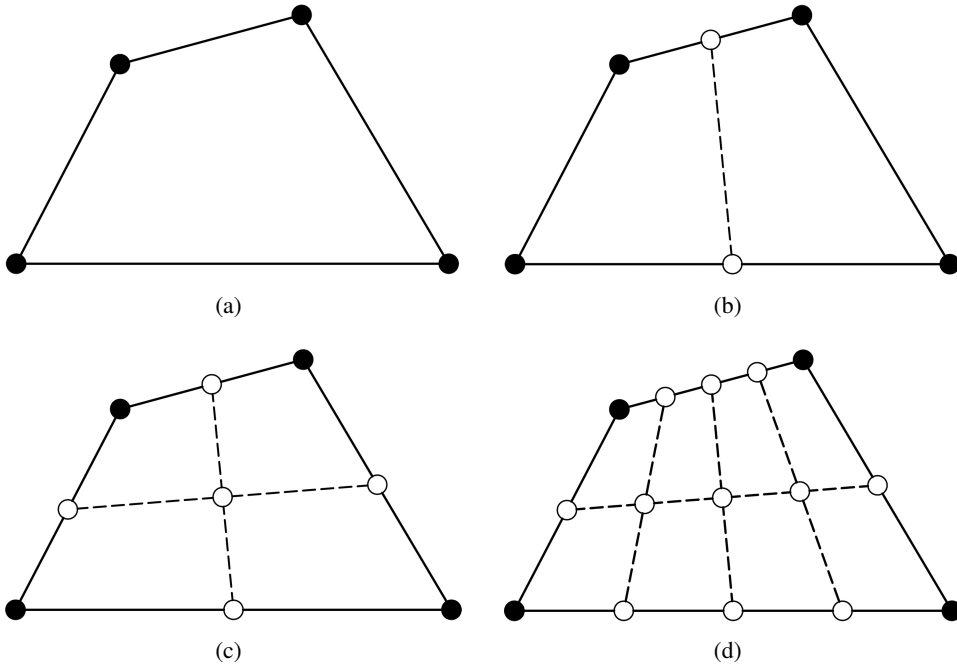

(a)

(b)

(c)

(d)

Figure 5: Smoothing domain (*SD*) concepts for the CS-FEM: (a) *1 SD*, (b) *2 SDs*, (c) *4 SDs,* and (d) *8 SDs*, see Liu, Nguyen X.H. and Nguyen T.T. (2010).

For each smoothing domain ($\Omega^{(c)}$) associated with a cell (c), the smoothed strains ($\tilde{\mathbf{S}}$) and smoothed electric fields ($\tilde{\mathbf{E}}$) for a piezoelectric structure can be written as:

$$\tilde{\mathbf{S}} = \int_{\Omega^{(c)}} \mathbf{S}(x)\chi^{(c)}(\mathbf{x})\mathrm{d}\Omega \tag{24}$$

$$\tilde{\mathbf{E}} = \int_{\Omega^{(c)}} \mathbf{E}(\mathbf{x})\chi^{(c)}(\mathbf{x})\mathrm{d}\Omega \tag{25}$$

where $\chi^{(c)}(\mathbf{x})$ is a smoothing function, simply chosen as:

$$\chi^{(c)}(\mathbf{x}) = \begin{cases} \frac{1}{A^{(c)}}, & x \in \Omega^{(c)} \\ 0, & x \notin \Omega^{(c)} \end{cases} \tag{26}$$

where $A^{(c)}$ is the area of the smoothing cell ($\Omega^{(c)}$) constructed by:

$$A^{(c)} = \int_{\Omega^{(c)}} \mathrm{d}\Omega. \tag{27}$$

Each element area is the summation of element cells areas, so:

$$A^e = \sum_c^{nSC} A_c \tag{28}$$

where *nSC* is the number of constructed cells for each element. Using the smoothing function (Eq. (26)) and by applying the divergence theorem, the smoothed strain and electric field will be changed to, see Liu, Nguyen X.H. and Nguyen T.T. (2010):

$$\tilde{\mathbf{S}} = \frac{1}{A^{(c)}} \int_{\Gamma^{(c)}} \mathbf{n}_u^{(c)}\mathbf{u}(\mathbf{x})\mathrm{d}\Gamma = \sum_{I \in N_n} \tilde{\mathbf{B}}_{u\,I}(\mathbf{x}_c)\mathrm{d}_I \tag{29}$$

$$\tilde{\mathbf{E}} = -\frac{1}{A^{(c)}} \int_{\Gamma^{(c)}} \mathbf{n}_\varphi^{(c)}\varphi(\mathbf{x})\mathrm{d}\Gamma = -\sum_{I \in N_n} \tilde{\mathbf{B}}_{\varphi\,I}(\mathbf{x}_c)\varphi_I \tag{30}$$

where $\Gamma^{(c)}$ is the boundary of the smoothing cell ($\Omega^{(c)}$), N_n is the number of element nodes, $\tilde{\mathbf{B}}_{u\,I}(\mathbf{x}_c)$ and $\tilde{\mathbf{B}}_{\varphi\,I}(\mathbf{x}_c)$ are the smoothed strain and smoothed electric field matricses on the domain ($\Omega^{(c)}$), respectively, and $\mathbf{n}_u^{(c)}$ and $\mathbf{n}_\varphi^{(c)}$ are the normal outward vectors on the boundary ($\Gamma^{(c)}$), such that:

$$\mathbf{n}_u^{(c)} = \begin{bmatrix} \mathbf{n}_x^{(c)} & 0 \\ 0 & \mathbf{n}_y^{(c)} \\ \mathbf{n}_y^{(c)} & \mathbf{n}_x^{(c)} \end{bmatrix}, \quad \mathbf{n}_\varphi^{(c)} = \begin{bmatrix} \mathbf{n}_x^{(c)} & \mathbf{n}_y^{(c)} \end{bmatrix}^{\mathrm{T}}. \tag{31}$$

Note that the values of $\tilde{\mathbf{B}}_{uI}(\mathbf{x}_c)$ and $\tilde{\mathbf{B}}_{\varphi I}(\mathbf{x}_c)$ are:

$$
\tilde{\mathbf{B}}_{uI}(\mathbf{x}_c) = \frac{1}{A^{(c)}}
\begin{bmatrix}
\int\limits_{\Gamma_b^{(c)}} \mathbf{N}_I \mathbf{n}_x d\Gamma & 0 \\
0 & \int\limits_{\Gamma_b^{(c)}} \mathbf{N}_I \mathbf{n}_y d\Gamma \\
\int\limits_{\Gamma_b^{(c)}} \mathbf{N}_I \mathbf{n}_y d\Gamma & \int\limits_{\Gamma_b^{(c)}} \mathbf{N}_I \mathbf{n}_x d\Gamma
\end{bmatrix}
$$

$$
= \frac{1}{A^{(c)}} \sum_{b=1}^{nb}
\begin{bmatrix}
\mathbf{N}_I(\mathbf{x}_b^g)\mathbf{n}_x^{(c)}(\mathbf{x}_b^g) & 0 \\
0 & \mathbf{N}_I(\mathbf{x}_b^g)\mathbf{n}_y^{(c)}(\mathbf{x}_b^g) \\
\mathbf{N}_I(\mathbf{x}_b^g)\mathbf{n}_y^{(c)}(\mathbf{x}_b^g) & \mathbf{N}_I(\mathbf{x}_b^g)\mathbf{n}_x^{(c)}(\mathbf{x}_b^g)
\end{bmatrix} l_b^{(c)}
\tag{32}
$$

$$
\tilde{\mathbf{B}}_{\varphi I}(\mathbf{x}_c) = \frac{1}{A^{(c)}}
\begin{bmatrix}
\int\limits_{\Gamma^{(c)}} \mathbf{N}_I \mathbf{n}_x d\Gamma \\
\int\limits_{\Gamma^{(c)}} \mathbf{N}_I \mathbf{n}_y d\Gamma
\end{bmatrix}
= \frac{1}{A^{(c)}} \sum_{b=1}^{nb}
\begin{bmatrix}
\mathbf{N}_I(\mathbf{x}_b^g)\mathbf{n}_x^{(c)}(\mathbf{x}_b^g) \\
\mathbf{N}_I(\mathbf{x}_b^g)\mathbf{n}_y^{(c)}(\mathbf{x}_b^g)
\end{bmatrix} l_b^{(c)}
\tag{33}
$$

where nb is the total number of boundary sections of $(\Gamma_b^{(c)})$, $\mathbf{x}_b^g$ is the midpoint(Gauss point) of each smoothing domain boundary segment $(\Gamma_b^{(c)})$, and $l_b^{(c)}$ is the length of each segment of $(\Gamma_b^{(c)})$. These equations show that unlike the standard FEMs, CS-FEM does not use the derivative of the shape functions for computing the smoothing (gradiant) strain and electric field matrices.

Similar to the standard FEM by applying Hamilton's principle, the general S-FEM discretized matrix form in a smoothing space $(\tilde{\cdot})$ will be changed to:

$$
\tilde{\mathbf{M}}(\rho)\ddot{\hat{\mathbf{d}}} + \tilde{\mathbf{C}}(\rho)\dot{\hat{\mathbf{d}}} + \tilde{\mathbf{K}}(\rho)\hat{\mathbf{d}} = \hat{\mathbf{P}}(\rho,t).
\tag{34}
$$

With a proportional damping assumption, the smoothing stiffness martix $(\tilde{\mathbf{K}})$ smoothing mass matrix $(\tilde{\mathbf{M}})$ and smoothing damping matrix $(\tilde{\mathbf{C}})$ will then become:

$$
\tilde{\mathbf{K}} =
\begin{bmatrix}
\tilde{\mathbf{k}}_{uu} & \tilde{\mathbf{k}}_{u\varphi} \\
\tilde{\mathbf{k}}_{u\varphi} & \tilde{\mathbf{k}}_{\varphi\varphi}
\end{bmatrix}; \quad
\tilde{\mathbf{M}} =
\begin{bmatrix}
\mathbf{m} & 0 \\
0 & 0
\end{bmatrix}; \quad
\tilde{\mathbf{C}} = \alpha\tilde{\mathbf{M}} + \vartheta\tilde{\mathbf{K}}.
\tag{35}
$$

The components of the smoothed stiffness matrix for each element domain can be calculated as follows, see Dai, Liu and Nguyen (2007):

$$
\tilde{\mathbf{K}}_{e(uu)} = \sum_c^{nSC} (\tilde{\mathbf{B}}_u^{(c)})^T c_E \tilde{\mathbf{B}}_u^{(c)} A^{(c)},
\tag{36}
$$

$$
\tilde{\mathbf{K}}_{e(u\varphi)} = \sum_c^{nSC} (\tilde{\mathbf{B}}_u^{(c)})^T e^T \tilde{\mathbf{B}}_\varphi^{(c)} A^{(c)},
\tag{37}
$$

$$\tilde{\mathbf{K}}_{e(\varphi\varphi)} = \sum_{c}^{nSC} (\tilde{\mathbf{B}}_{\varphi}^{(c)})^{\mathrm{T}} \varepsilon_s \tilde{\mathbf{B}}_{\varphi}^{(c)} A^{(c)}. \tag{38}$$

For a time-harmonic excitation problem, the load vector in Eq. (34) ($\hat{\mathbf{P}}(\rho,t)$) has the general form:

$$\hat{\mathbf{P}}(\rho,t) = \mathbf{f}(\rho)\mathrm{e}^{iwt} \tag{39}$$

where $\mathbf{f}(\rho)$ is the magnitude of the applied load vector, w is the rotational frequency of the applied load, and (i) is the imaginary number in complex variables. With this assumption, Eq. (34) can be converted to:

$$\tilde{\mathbf{M}}(\rho)\ddot{\hat{\mathbf{d}}} + \tilde{\mathbf{C}}(\rho)\dot{\hat{\mathbf{d}}} + \tilde{\mathbf{K}}(\rho)\hat{\mathbf{d}} = \mathbf{f}(\rho)\mathrm{e}^{iwt}. \tag{40}$$

Note that the steady sate solution of Eq. (40) is:

$$\hat{\mathbf{d}}(t) = \hat{\mathbf{u}}(\rho)\mathrm{e}^{iwt} \tag{41}$$

where $\hat{\mathbf{u}}(\rho)$ is the magnitude of the displacement vector in complex form. By this assumption, Eq. (40) yields:

$$\left[-w^2\tilde{\mathbf{M}}(\rho) + iw\tilde{\mathbf{C}}(\rho) + \tilde{\mathbf{K}}(\rho) \right] \hat{\mathbf{u}} = \mathbf{f}(\rho). \tag{42}$$

Then, by introducing a dynamic stiffness matrix ($\tilde{\mathbf{G}}(\rho,w)$), an alternative general form of this equation becomes:

$$\tilde{\mathbf{G}}(\rho,w)\hat{\mathbf{u}} = \mathbf{f}(\rho) \tag{43}$$

with:

$$\tilde{\mathbf{G}}(\rho,w) = -w^2\tilde{\mathbf{M}}(\rho) + iw\tilde{\mathbf{C}}(\rho) + \tilde{\mathbf{K}}(\rho). \tag{44}$$

After solving Eq. (43) through the CS-FEM analysis, the instantaneous displacement ($\mathbf{x}(t)$) and velocity ($\dot{\mathbf{x}}(t)$) can be respectively achieved as:

$$\mathbf{x}(t) = Real(\hat{\mathbf{u}}(\rho)\mathrm{e}^{iwt}), \tag{45}$$

$$\dot{\mathbf{x}}(t) = Real(iw\hat{\mathbf{u}}(\rho)\mathrm{e}^{iwt}). \tag{46}$$

As can be seen in the above equations, only the calculation of the stiffness matrix in the CS-FEM method is different from the standard FEM computations.

The solution of the CS-FEM with $nSC = 1$ is equal to the standard FEM solution using reduced integration points (upper bound solution with flexible stiffness). If the number of smoothed domains for each element approaches infinity, the solution will approach the full integration standard FEM solution with (2×2) Gauss integration (lower bound solution with stiff stiffness). Finally, if $1 < nSC < \infty$ the CS-FEM model is always softer than the FEM using the same set of elements, and the CS-FEM solution (in strain energy) falls between the upper-bound and lower-bound FEM solutions of the force driving problems, see Liu, Nguyen, Dai and Lam (2007). Since the displacement conformity in this method is only valid along the edges of each cell, the computed stiffness matrices and displacements obtained through this method will be more flexible and more accurate than the standard FEM values, respectively, see Chen, Wu and Yoon (2001); Liu, Dai and Nguyen (2007); Liu, Nguyen, Dai and Lam (2007). In particular, for nonlinear problems, computations through this method have a faster convergence rate than for standard FEMs, though its computation time is longer than the standard FEM analysis, see Liu, Dai and Nguyen (2007); Liu, Nguyen, Dai and Lam (2007). In addition, because the CS-FEM does not use derivatives of shape functions, it is a type of weak form method, see Liu (2009).

4   Reliability based topology optimization

The main aim of deterministic topology optimization (DTO) is to reduce costs without focusing on the effects of uncertainties in the materials, geometry, and loading. To improve this type of design, a RBTO analysis is required. The final optimized design obtained through this type of optimization will be safer and more reliable compared to DTO designs. The first step of the RBTO analysis is to find the effects of the considered uncertainties of the system. After computing the reliability design values, the topology optimization process will then be implemented.

4.1   Reliability evaluation

For a reliability analysis, the failure probability (P_f) of a system is generally calculated as, see Kharmanda, Olhoff, Mohamed and Lemaire (2004):

$$P_f = P_r\left[Li(\mathbf{X}, \mathbf{Y}) \leq 0\right] = \int\limits_{Li(\mathbf{x}, \mathbf{y}) \leq 0} f_Y(\mathbf{Y}) \mathrm{d}\mathbf{Y}_1 ... \mathrm{d}\mathbf{Y}_n \qquad (47)$$

where $(Li(\mathbf{X}, \mathbf{Y}) = 0)$ is the limit sate surface (function), $(Li(\mathbf{X}, \mathbf{Y}) \leq 0)$ expresses the state of failure for the system, and $(Li(\mathbf{X}, \mathbf{Y}) > 0)$ explains the state of the safety. In addition, $f_Y(\mathbf{Y})$ is the joint density function for the random variables $(\mathbf{Y}_i)$, $P_r[\cdot]$

is the probability operator, n is the number of random variables, and **X** is the design variable.

The reliability satisfying condition for a system can then be written as:

$$P_r[Li_i(\mathbf{X},\mathbf{Y}) \leq 0] - \Phi(-\beta_t) \leq 0 \; i = 1,...,np \tag{48}$$

where np, $\Phi(\cdot)$, and β_t are the number of probabilistic constraints, standard normal Gaussian cumulated function, and target reliability index, respectively.

Note that the normal distribution is expressed as:

$$\Phi(\mathbf{z}) = \frac{1}{\sqrt{2\pi}} \int\limits_{-\infty}^{z} e^{\frac{-z^2}{2}} \, dz. \tag{49}$$

In practice, probability approximation methods such as the first order reliability method (FORM) and the second order reliability method (SORM) are employed to calculate the failure probability, see Ditlevsen and Madsen (1996); Madsen, Krenk and Lind (1986). The FORM technique approximates a limit state function as a linear function, and this method usually has enough accuracy for optimization problems.

The original random variables (**Y**) in the FORM approximation should be transformed to normalized variables ($\boldsymbol{\mu}$) through a transformation function (T), see Rackwits and Fiessler (1978); Hohenbichler and Rackwitz (1981):

$$\boldsymbol{\mu} = T(\mathbf{X},\mathbf{Y}) \text{ and } \mathbf{Y} = T^{-1}(\mathbf{X},\boldsymbol{\mu}). \tag{50}$$

A common normalized random variable form can then be written as:

$$\boldsymbol{\mu}_i = \frac{\mathbf{Y}_i - Mean_i}{\sigma_i} \; , i = 1,2,...,nr \tag{51}$$

where $Mean_i$, σ_i, and nr are the mean value of the (i^{th}) random variable , standard deviation, and the number of random variables, respectively.

A transformation tool will map the limit state function in the original domain ($Li(\mathbf{X},\mathbf{Y})$) to the normal domain ($H(\mathbf{X},\boldsymbol{\mu})$), such that:

$$H(\mathbf{X},\boldsymbol{\mu}) \equiv Li(\mathbf{X},\mathbf{Y}) = 0. \tag{52}$$

By supposing a FORM technique and using the reliability index for a system, the failure probability of this system will be approximated easier than the Eq. (47), see Kharmanda, Olhoff, Mohamed and Lemaire (2004), i.e.,

$$P_f \approx \Phi(-\beta) \tag{53}$$

where β is the reliability index. The reliability index concept was first introduced by Hasofer and Lind in 1974; this index is defined as the minimum distance of the origin with respect to the limit state function in a normal space (figure 6). Thus,

$$\beta = Min(\boldsymbol{\mu}^{\mathrm{T}}\boldsymbol{\mu})^{\frac{1}{2}} \; sbujectto : \; H(\mathbf{X},\boldsymbol{\mu}) = 0. \tag{54}$$

Figure 6 presents some of the reliability concepts in further detail; see Kim, Wang, Hwang and Lee (2005).

Based on the FORM technique assumption, there are usually two approaches for finding the reliability of a system, see Kharmanda, Olhoff, Mohamed and Lemaire (2004):

a. Reliability Index Approach (RIA).

b. Performance Measure Approach (PMA).
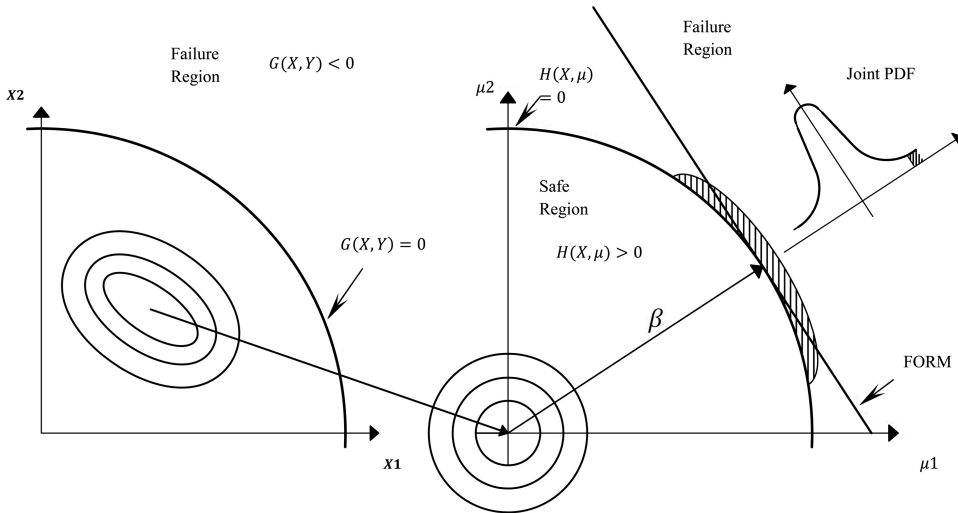
Figure 6: Concepts of reliability design optimization and FORM approximation, see Kim, Wang, Hwang and Lee (2005).

4.1.1 First order reliability analysis in RIA

In this method, the system reliability index (β) is obtained by solving the optimization problem:

$$RIA : \begin{cases} Minimize : \; \|\boldsymbol{\mu}\| \\ Constraint : H(\mathbf{X},\boldsymbol{\mu}) = 0 \end{cases}, \tag{55}$$

and the reliability of a system can be computed according to the Eq. (56),such that:

$$\beta = Min(\boldsymbol{\mu}^{\mathrm{T}}\boldsymbol{\mu})^{\frac{1}{2}} \ sbujectto: H(\mathbf{X},\boldsymbol{\mu}) = 0 \ or \ \beta = \left\|\boldsymbol{\mu}^*_{H(\mathbf{X},\boldsymbol{\mu})=0}\right\| \tag{56}$$

where $\boldsymbol{\mu}^*$ is the random variable design point and this point is obtained from the solution of Eq. (55).

4.1.2   First order reliability analysis in PMA

Similar to the RIA method, the random design variable values ($\mu^*_{\beta=\beta_t}$) can be obtained by solving the optimization problem:

$$PMA: \begin{cases} Minimize: \ H(\mathbf{X},\boldsymbol{\mu}) \\ Constraint: \ \|\boldsymbol{\mu}\| = \beta_t \end{cases}. \tag{57}$$

In order to determine the random design points, the advanced mean value (AMV) method has been recognized being more efficient than other optimization algorithms, see Wu (1994).

The sensitivity analysis of some considered uncertainty constraints during the RBTO procedure is essential, and therefore the implementation of the PMA is usually preferred, see Kim, Wang, Bae and Moon (2006).

4.1.2.1 Advanced mean value method

This optimization method searches the direction of the steepest descent vector to find the random design points, see Youn, Choi and Park (2003). This technique is always stable and efficient for a convex set.

The AVM is defined as an iterative procedure with the following first suggestion point:

$$\boldsymbol{\mu}^*_{MVi} = \beta_t \mathbf{n}_i(0) \tag{58}$$

where

$$\mathbf{n}_i(0) = -\frac{\nabla_\mu H(\mathbf{X},\boldsymbol{\mu}_i = 0)}{\left\|\nabla_\mu H(\mathbf{X},\boldsymbol{\mu}_i = 0)\right\|}$$

where i is the number of considered probabilistic constraints.

Updating algorithm for the kth iteration can be formulated as:

$$\boldsymbol{\mu}^{(1)}_{AMVi} = \boldsymbol{\mu}^*_{MVi} \ ; \ \boldsymbol{\mu}^{(k+1)}_{AMVi} = \beta_t \mathbf{n}_i(\mu^{(k)}_{AMV}) \tag{59}$$

where:

$$\mathbf{n}_i(\boldsymbol{\mu}_{AMV}^{(k)}) = -\frac{\nabla_\mu H(\mathbf{X}, \boldsymbol{\mu}_{AMV}^{(k)})}{\left\|\nabla_\mu H(\mathbf{X}, \boldsymbol{\mu}_{AMV}^{(k)})\right\|}, \tag{60}$$

and $\mathbf{n}(\cdot)$ is the normalized steepest descent direction.

Figure 7 provides more detailed information about this procedure; see Luo Y., Kang, Luo Z. and Li (2009).
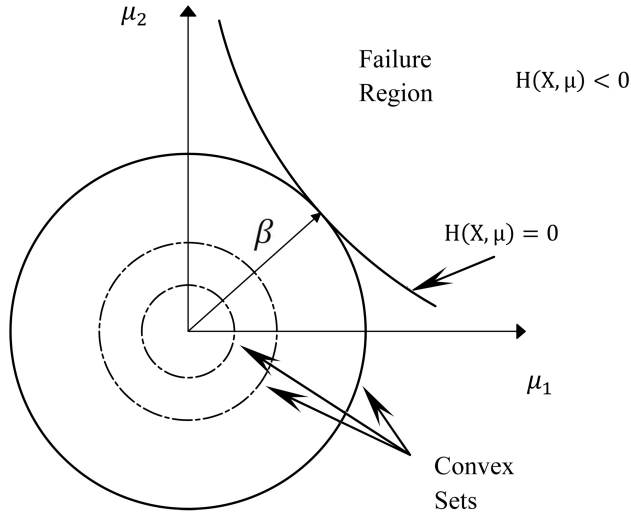

Figure 7: PMA concept for reliability analysis, see Luo Y., Kang, Luo Z. and Li (2009).

4.2 Topology optimization procedure

This technique determines the optimum material distribution for a system to optimize an objective function, such as velocity, with respect to some defined constraints.

The general forms of DTO and RBTO problems are, see Youn, Choi and Park (2003):

$$DTO: \begin{cases} \text{Optimize : an objective function} \\ \text{Constraints :} \begin{cases} \text{Equilibrium equations} \\ \text{Volume, cost or certainty constraints} \end{cases} \end{cases} \tag{61}$$

and

$$RBTO: \begin{cases} \text{Optimize : an objective function} \\ \text{Constraints :} \begin{cases} \text{Equilibrium equations} \\ \text{Volume, cost or certainty constraints} \\ \text{Uncertainty or reliability constraints(RIA or PMA)} \end{cases} \end{cases}.$$

(62)

Numerical approaches such as homogenization, see Bendsoe and Kikuchi (1988), and SIMP techniques, see Rozvany, Zhou and Birker (1992); Bendsoe (1989), are commonly used to determine topology optimization designs. The homogenization model uses microscopic material distribution to find the optimum solution, whereas the SIMP method employs the pseudo density of each element as a design variable. Since the SIMP method implementation is relatively simpler and is more efficient than the homogenization model, this algorithm is usually preferred.

The SIMP technique can be successfully applied for multi-constraints, multi-materials, and multi- physics conditions. Through this method, the intermediate densities of each element (pseudo density (ρ_e)) are penalized to distinctive values near 0 (void) or 1 (solid), see Bendsoe and Sigmund (2003).

For an isotropic material, each element's Young's modulus matrix ($\mathbf{E}_e(\rho_e)$) is approximated as:

$$\mathbf{E}_e(\rho_e) = (\rho_e)^p \mathbf{E}_e^0; \quad 0 < \rho_{min} \leq \rho_e \leq 1$$

(63)

where $\mathbf{E}_e^0$ and p are each element's Young's modulus matrix for a solid state material($\rho_e = 1$) and penalization factor, respectively. The minimum density value ($\rho_{min} = 0.01$) is mentioned in Eq. (63) in order to avoid singularity of the stiffness matrix during the FEM solution.

For a dynamic system, a mass matrix ($\mathbf{M}_e(\rho_e)$) is approximated as, see Du and Olhoff (2007):

$$\mathbf{M}_e(\rho_e) = (\rho_e)^q \mathbf{M}_e^0$$

(64)

where $\mathbf{M}_e^0$ represents the element mass matrix corresponding to the solid state material, and q is the penalization factor for the mass matrix (usually equal to 1).

For piezoelectric structures, these interpolations are applied on the three elements (c_E), (e), and (ε_s) (according to Eq. (2)) as, see Kim J.E., Kim D.S., Ma and Kim Y.Y. (2010):

$$c_E = f_c(\rho_e) c_E^0$$

(65)

$$e = f_e(\rho_e)e^0 \tag{66}$$

$$\varepsilon_s = f_\varepsilon(\rho_e)\varepsilon_s^0 \tag{67}$$

where f_c, f_e, and f_ε are the material coefficient interpolation functions, and c_E^0, e^0, and ε_s^0 represent the nominal material matrices for the solid material case $(\rho_e = 1)$. Based on the piezoelectric material with penalization and polarization (PEMAP-P) model, these interpolation coefficients can be written as, see Kim J.E., Kim D.S., Ma and Kim Y.Y. (2010):

$$f_c(\rho_e) = \rho_e^{nc}; \quad f_e(\rho_e) = \rho_e^{ne}; \quad f_\varepsilon(\rho_e, \gamma_e) = \rho_e^{n\varepsilon}(2\gamma_e - 1)^{np} \tag{68}$$

where the exponents *nc*, *ne*, and *nε* are the material density penalization factors, and *np* is the penalization power for the polarization variable (γ_e). By ignoring the effect of polarization, this equation leads to; see Kim J.E., Kim D.S., Ma and Kim Y.Y. (2010):

$$f_c(\rho_e) = \rho_e^{nc}; \quad f_e(\rho_e) = \rho_e^{ne}; \quad f_\varepsilon(\rho_e) = \rho_e^{n\varepsilon}. \tag{69}$$

Finding appropriate penalization powers is usually based on a trial and error process; see Bendsoe and Sigmund (1999). To respectively achieve a black and white configuration for these types of structures, Kim J.E., Kim D.S., Ma and Kim Y.Y. in 2010 derived some relations between these exponents for a static condition as:

$$2n\varepsilon - (nc + ne) > 0, \tag{70}$$

$$n\varepsilon - nc > 0. \tag{71}$$

4.3 Sensitivity analysis

The sensitivity analysis is usually a critical procedure in optimization problems. Since reliability and topology optimization have been considered as independent processes in this work, the evaluation of two sensitivities is essential; the first relates to the reliability process and the second relates to the topology optimization process.

4.3.1 Sensitivity analysis for reliability process

Random variables do not usually have the same effects on the reliability of a system. Therefore, to quantitatively find the effects of these variables, sensitivity of the limit state function $(Li(\mathbf{X}, \mathbf{Y}))$ (such as stiffness, compliance, displacement or eigenfrequency) with respect to the considered random variables (such as load, thickness or material properties) should be conducted.

The forward finite difference method (FFD) is an acceptable choice for this task; see Kharmanda, Olhoff, Mohamed and Lemaire (2004). This method is formulated as:

$$\frac{\partial(Li)}{\partial(Mean_i)} = \frac{Li(Mean_i + \Delta Mean_i) - Li(Mean_i)}{\Delta Mean_i} \tag{72}$$

where $Mean_i$ is the mean value of the (i^{th}) random variable, and $\Delta Mean_i$ is an allowable variation of this amount, such that:

$$\frac{\Delta Mean_i}{Mean_i} = 0.001 \tag{73}$$

Similar to this calculation, the sensitivity analysis inside the AMV optimizer can be successfully handled by the FFD method.

4.3.2 Sensitivity analysis for topology optimization process

During the design variable updating process (such as the MMA optimizer), calculation of the objective function (*Object Fun*) and related constraints differentiations with respect to design variables (ρ_e) is necessary. Here, this sensitivity analysis is conducted via an efficient method called the adjoint sensitivity analysis; see Choi and Kim (2005).

For a dynamic system, an objective function can be defined using a real function (*Object Fun*$_0$) as, see Jensen (2009):

$$Object\ Fun = Object\ Fun_0(\rho, \hat{\mathbf{u}}_r, \hat{\mathbf{u}}_i) \tag{74}$$

where $\hat{\mathbf{u}}_r$ and $\hat{\mathbf{u}}_i$ are the real part and imaginary parts of the displacement vector, respectively. By introducing the Lagrangian multiplier ($\boldsymbol{\lambda}$), the adjoint form of this function becomes:

$$Object\ Fun = Object\ Fun_0(\rho, \hat{\mathbf{u}}_r, \hat{\mathbf{u}}_i) + \boldsymbol{\lambda}^{\mathrm{T}}(\tilde{\mathbf{G}}\hat{\mathbf{u}} - \mathbf{f}) + \bar{\boldsymbol{\lambda}}^{\mathrm{T}}(\bar{\tilde{\mathbf{G}}}\bar{\hat{\mathbf{u}}} - \bar{\mathbf{f}}) \tag{75}$$

where the over bar items in Eq.(75) denote the complex conjugates.

Based on Jensen's note in 2009, the final sensitivity expression then is:

$$\frac{\mathrm{d}(Object\ Fun)}{\mathrm{d}\rho_e} = \frac{\partial(Object\ Fun_0)}{\partial\rho_e} + 2Real\left[\boldsymbol{\lambda}^{\mathrm{T}}(\frac{\partial\tilde{\mathbf{G}}}{\partial\rho_e}\hat{\mathbf{u}} - \frac{\partial\mathbf{f}}{\partial\rho_e})\right] \tag{76}$$

where ($\boldsymbol{\lambda}$) is the solution to:

$$\tilde{\mathbf{G}}\boldsymbol{\lambda} = -\frac{1}{2}\left[\frac{\partial(Object\ Fun_0)}{\partial\hat{\mathbf{u}}_r} - \mathrm{i}\frac{\partial(Object\ Fun_0)}{\partial\hat{\mathbf{u}}_i}\right]^{\mathrm{T}}. \tag{77}$$

For these systems:

$$\frac{\partial \tilde{\mathbf{G}}}{\partial \rho_e} = -w^2 \frac{\partial \tilde{\mathbf{M}}}{\partial \rho_e} + \mathrm{i}w \frac{\partial \tilde{\mathbf{C}}}{\partial \rho_e} + \frac{\partial \tilde{\mathbf{K}}}{\partial \rho_e}. \tag{78}$$

The components of this equation for piezoelectric materials and by a proportional damping assumption can be approximated by the SIMP method as, see Kim J.E., Kim D.S., Ma and Kim Y.Y. (2010); Du and Olhoff (2007):

$$\frac{\partial \tilde{\mathbf{M}}}{\partial \rho_e} = \begin{cases} \tilde{\mathbf{M}}_e^0 & \rho_e > 0.1 \\ 6c_0 \rho_e^5 \tilde{\mathbf{M}}_e^0 & \rho_e \le 0.1 \ (c_0 = 10^5) \end{cases} \tag{79}$$

$$\frac{\partial \tilde{\mathbf{K}}}{\partial \rho_e} = \begin{bmatrix} \frac{\partial \tilde{\mathbf{K}}_{e(uu)}}{\partial \rho_e} & \frac{\partial \tilde{\mathbf{K}}_{e(u\varphi)}}{\partial \rho_e} \\ \frac{\partial \tilde{\mathbf{K}}_{e(u\varphi)}}{\partial \rho_e} & \frac{\partial \tilde{\mathbf{K}}_{e(\varphi\varphi)}}{\partial \rho_e} \end{bmatrix} = \begin{bmatrix} nc(\rho_e)^{nc-1}\tilde{\mathbf{K}}_{e(uu)}^0 & ne(\rho_e)^{ne-1}\tilde{\mathbf{K}}_{e(u\varphi)}^0 \\ ne(\rho_e)^{ne-1}\tilde{\mathbf{K}}_{e(u\varphi)}^0 & n\varepsilon(\rho_e)^{n\varepsilon-1}\tilde{\mathbf{K}}_{e(\varphi\varphi)}^0 \end{bmatrix} \tag{80}$$

$$\frac{\partial \tilde{\mathbf{C}}}{\partial \rho_e} = \alpha \frac{\partial \tilde{\mathbf{M}}}{\partial \rho_e} + \vartheta \frac{\partial \tilde{\mathbf{K}}}{\partial \rho_e} \tag{81}$$

where $(\tilde{\cdot})_e^0$ denotes the element stiffness or mass smoothed matrices for the solid material sate.

5   Problem algorithm

The applied PBTO algorithm for this study can be summarized in figure 8.

6   Numerical results and discussions

DTO and RBTO numerical results of the prescribed mechanism (according to figures 2-4) for various numerical methods will be examined and compared here, with some of these results further discussed at the end of this section. All computations were conducted on a PC using an *Intel® Core(TM) 2 Quad*, Q9550@2.83 *GHZ CPU*, and *4GB RAM*.

6.1   Numerical results

6.1.1   Problem definition

The final goal of this study is to find an optimal material distribution required for a linear micromotor (shown in figure 2) to reach the maximum linear velocity. To that end, a set of proper objective function and constraints need to be defined.

According to Eq. (46) (for a constant excitation frequency), if the resultant end-point displacement for each beam is maximized, the end-point velocity of this beam
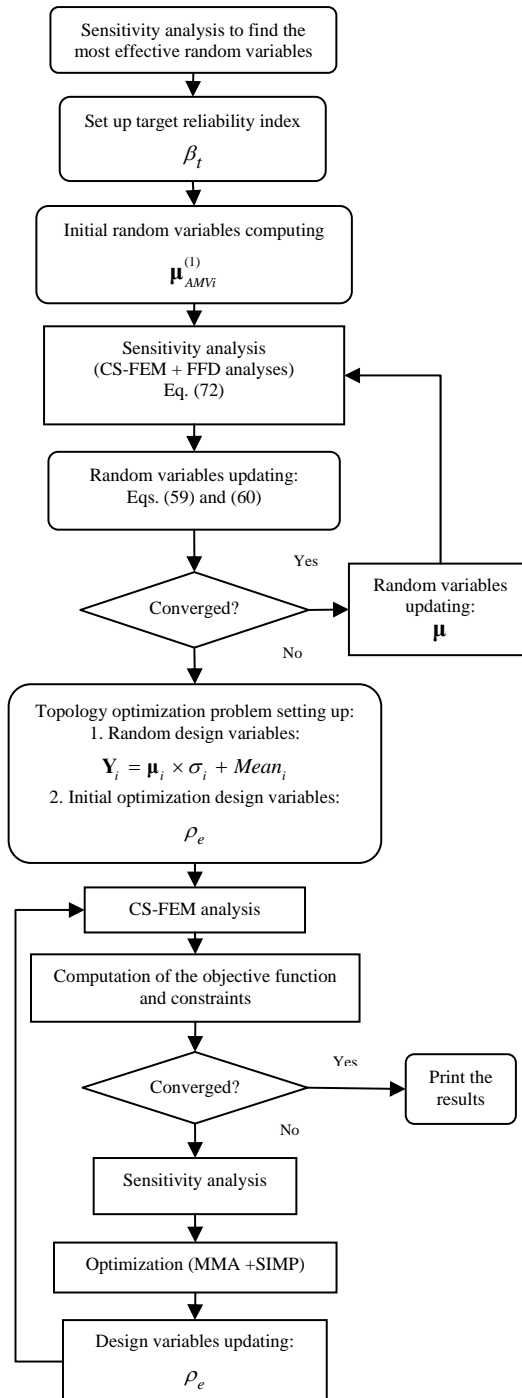
Figure 8: General applied RBTO flow chart for this study.

will be maximized. Hence, the final objective function can be defined to maximize resultant end-point displacement of each microbeam (point (A) in figure 9 (b)). The matrix form of the objective function can thus be written as:

$$Object\ Fun_0 = -\hat{\mathbf{u}}^T \mathbf{L} \bar{\hat{\mathbf{u}}} \tag{82}$$

where $\mathbf{L}$ is a diagonal matrix independent from the design variable whose non-zero diagonal entries are proportional to the position of point (A) in figure 9 (b).

The configuration (including materials and polarization direction), design domain, and dimension of each beam are shown in figures 9 (a), 9(b) and 10. The thickness of each beam is 1 (mm), applied voltage is 100 (volts) ($\mathbf{V_0} = 100(v)$), and the excitation frequency w is 1 Hz.

(a)

(b)
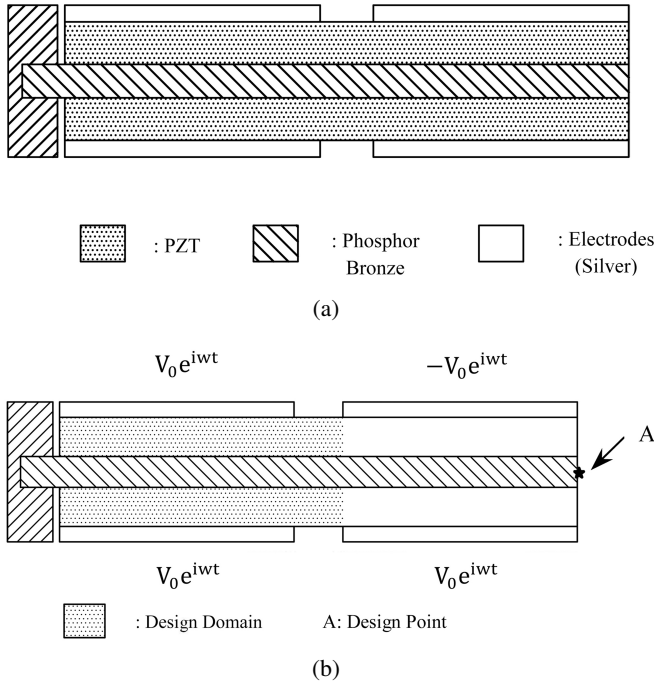
Figure 9: Definition of the problem: (a) general configuration and (b) design domain.

The setting of this problem can be summarized as follows:

$$\begin{cases} Objective\ function : -\hat{\mathbf{u}}^T \mathbf{L} \bar{\hat{\mathbf{u}}} \\ Design\ variable : Pesudo\ density(\rho_e) \\ Random\ variables : Voltage;\ thickness;\ matrial\ properties\ of\ piezoelectric\ layers \end{cases}$$
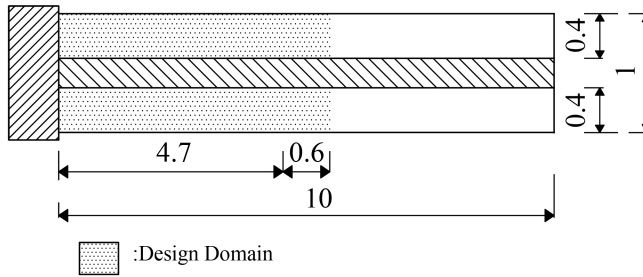
Figure 10: Dimension of the optimization problem (based on mm).

$$(83)$$

and

$$Subject\ to:\begin{cases} Equilibrium\ equations \\ \dfrac{\sum\limits_{e=1}^{num} Vol_e(\rho_e)}{Vol_0} \leq volfrac = 50\% \\ Minimize: \begin{cases} H(\rho_e, \boldsymbol{\mu}) \\ constraint: \|\boldsymbol{\mu}\| = \beta_t \end{cases} \\ 0 < \rho_{min} \leq \rho_e \leq 1 \end{cases} \qquad (84)$$

where Vol_0, Vol_e, num, and are the volume of the design domain corresponding to $\rho_e = 1$, volume of each element, number of elements in the design domain, and the volume fraction ratio, respectively.

This problem is then analyzed using the following assumptions and parameters:

a. The problem condition is linear and quasi-static.

b. The thickness of each electrode is very small in comparison to dimensions of the other parts.

c. The failure probability of 0.135% ($\beta_t = 3$) is considered as an uncertainty constraint.

d. A mesh of elements is used.

e. Material properties of the PZT are obtained from reference; see Nguyen X.H., Liu, Nguyen T.T. and Nguyen C.T. (2009).

6.1.2   Reliability analysis results

The first step for our reliability evaluation procedure is finding the most effective random variables. This is accomplished by sensitivity analyses of the limit state

function (displacement) respect to all the random variables under consideration. The results of these sensitivity analyses are summarized in table 1.

Table 1: Sensitivity analyses of displacement with respect to random variables.

Random variables	FEM method	FEM method	FEM method	FEM method	FEM method
	T3-FEM	Q4-FEM	CS-FEM (nSD=2)	CS-FEM (nSD=4)	CS-FEM (nSD=8)
Applied voltage	4.18E04	4.33E04	4.41E04	4.35E04	4.33E04
Thickness	1.21E-07	3.17E-08	3.8E-08	4.25E-08	2.88E-08
Elastic material property	-718	-409.19	-257.06	-390	-399.63
Piezoelectric material property	1.07E-13	1.16E-13	1.2E-13	1.16E-13	1.16E-13
Dielectric material property	-3.76E-06	-2.77E-06	-2.72E-06	-2.77E-06	-2.77E-06

It is clear that the applied voltage and elastic material property of the piezoelectric layers affect most effective on the limit state function. Hence, these two variables should be analyzed through the PMA and AVM to determine random design points. To start this process, first these random variables should be normalized using a suitable transform function (Eq. (51)). For this case, 10% deviation has been allowed for the mean values. After finding design values for the applied voltage and material properties, topology optimization process is started.

6.1.3 Topology optimization results

Using Eqs. (76) and (77), a sensitivity analysis for the above objective function (Eq. (82)) is calculated via the adjoint variable method as:

$$\frac{\mathrm{d}(-\hat{\mathbf{u}}^T \mathbf{L}\bar{\hat{\mathbf{u}}})}{\mathrm{d}\rho_e} = -2Real(\boldsymbol{\lambda}^T \frac{\partial \tilde{\mathbf{G}}}{\partial \rho_e}\hat{\mathbf{u}}) \tag{85}$$

and

$$\tilde{\mathbf{G}}\lambda = \mathbf{L}^T \bar{\hat{\mathbf{u}}} \tag{86}$$

6.1.3.1 DTO ($\beta_t = 0$) analysis with 50% volume fraction

This optimization is performed with 50% failure probability, and the topology optimization results obtained using our procedure are listed in table 2.

Table 2: Comparisons of our DTO designs with 50% volume fraction.

FEM method	Initial instantaneous velocity (mms^{-1})	Optimized instantaneous velocity (mms^{-1})	Number of iterations	Total CPU time (min)
Q4-FEM	0.0297	1.0625	278	60.0
T3-FEM	0.0249	0.7045	249	51.0
CS-FEM (*nSD=2*)	0.0329	1.4668	282	56.8
CS_FEM (*nSD=4*)	0.0304	1.1393	367	101.7
CS_FEM (*nSD=8*)	0.0299	1.1183	218	79.9

The instantaneous velocity convergence rates and our DTO configurations are found using the different approaches, as shown in figures 11 (a) to 11(e) and figures 12 (a) to 12(e).

6.1.3.2 RBTO ($\beta_t = 3$) analysis with 50% volume fraction

Considering now the uncertainty constraints, topology optimization designs will be examined here. If the target reliability index is chosen based on 0.1355% failure probability ($\beta_t = 3$), the topology optimization designs at the mean random values are listed in table 3.

The instantaneous velocity convergence rates and our RBTO designs (at the mean random values) are found using different FEM techniques, as shown in the figures 13 (a) to 13(e) and figures 14 (a) to 14(e).

6.2 Reanalysis

Since topology optimization designs usually include gray zones (as can be observed in figures 12 and 14), these structures are not generally suitable for manufacturing. To improve this defect, a reanalysis process is executed at the end of the optimization procedure; see Bendsoe and Sigmund (2003). By applying this technique, the design variables (e.g., the pseudo density of each element) that are less than a threshold factor will be removed and the larger values will be approximated as the
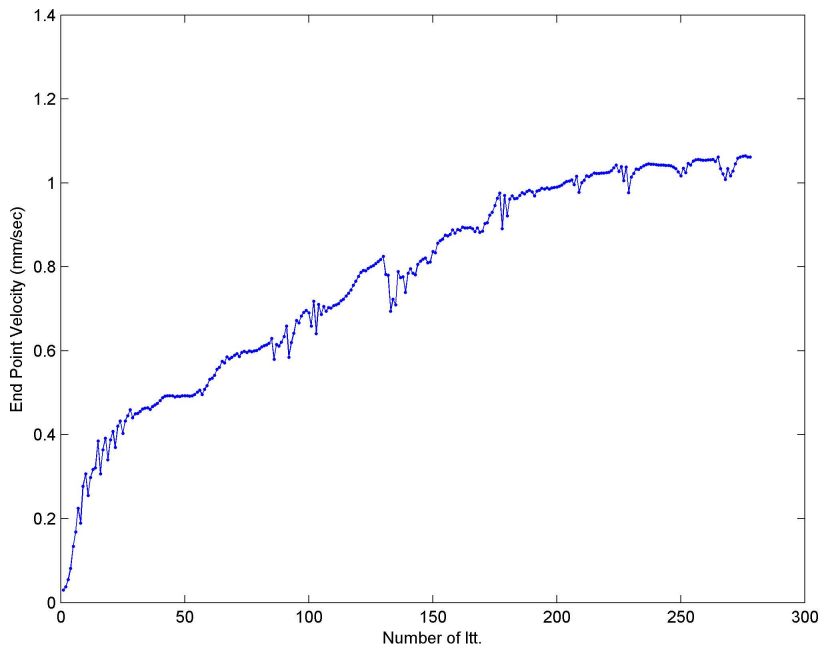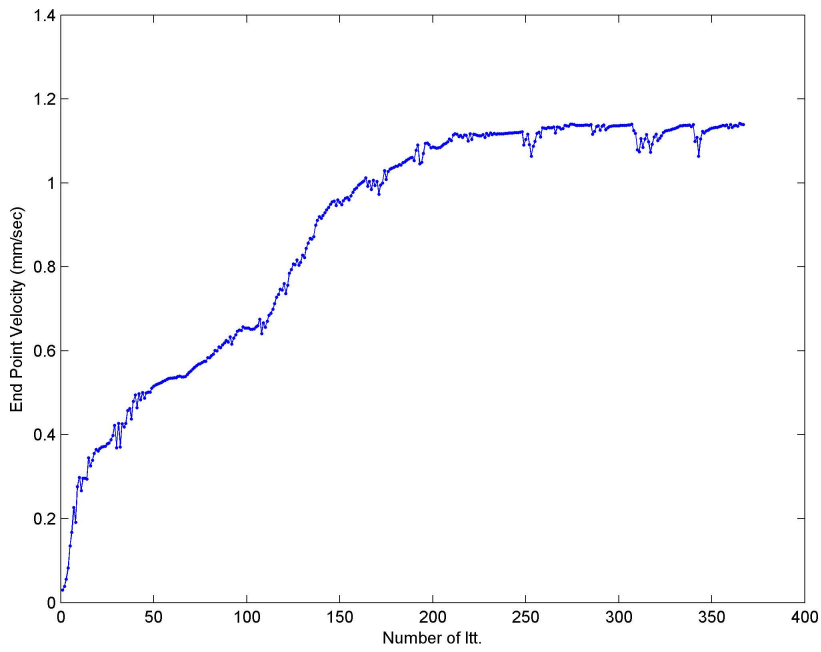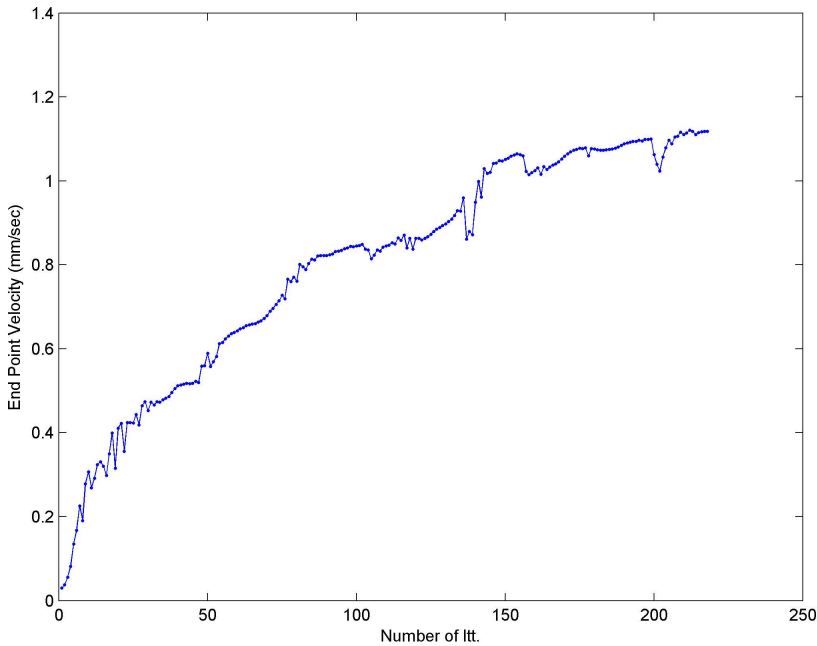
(a)
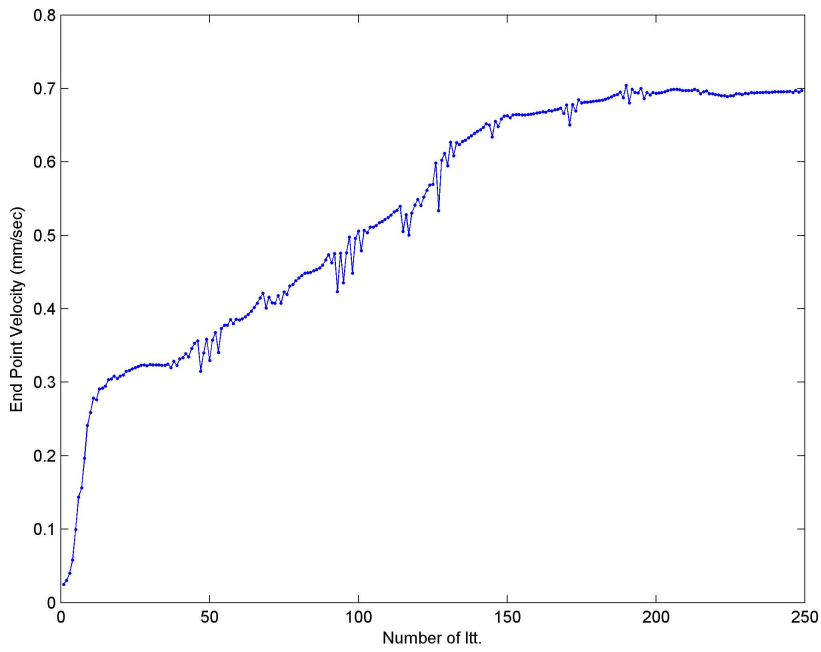
(b)
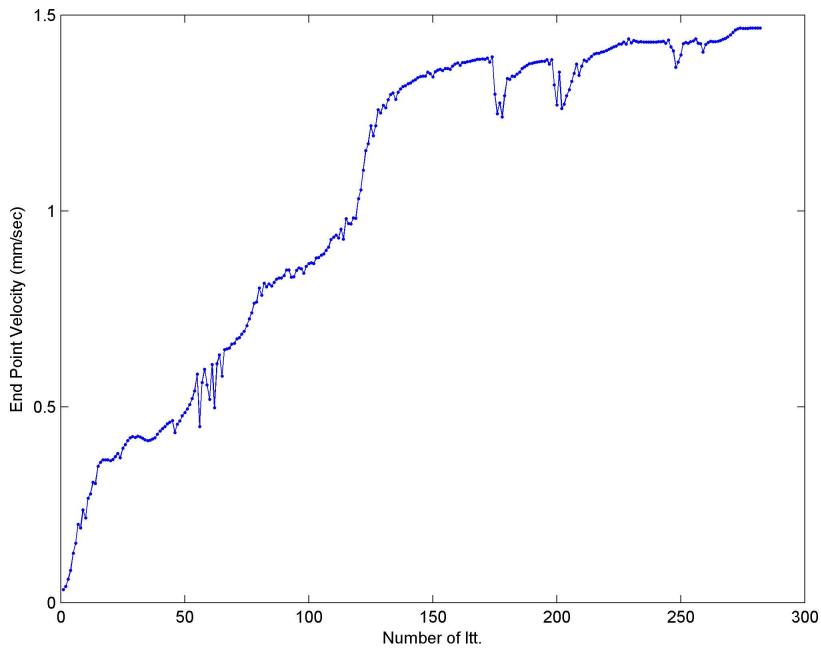
(c)

(d)

(e)

Figure 11: DTO designs' velocity convergence rates (50% volume fraction) for: (a) Q4-FEM, (b) T3-FEM, (c) CS-FEM (*nSD=2*), (d) CS-FEM (*nSD=4*), and (e) CS-FEM (*nSD=8*).

solid state condition ($\rho_e = 1$).Based on this procedure, our final DTO and RBTO results are listed in table 4, where the threshold factor is 0.6.

The reanalysis configurations for our DTO and RBTO (for 0.6 threshold factor) are shown in figures 15 (a) to 15(e) and figures 16(a) to 16(e).

For better comparison, the DTO and RBTO reanalysis results are collected again in table 5 in summary (threshold factor: 0.6).

6.3 Discussions

It has been known that when the number of smoothing domains increases, the CS-FEM approaches the Q4-FEM results, see Liu, Dai and Nguyen (2007); Liu and Nguyen (2010); Liu, Nguyen, Dai and Lam (2007). This was also observed in the final RBTO and DTO results: when the number of smoothing domains was
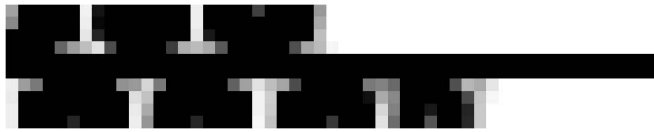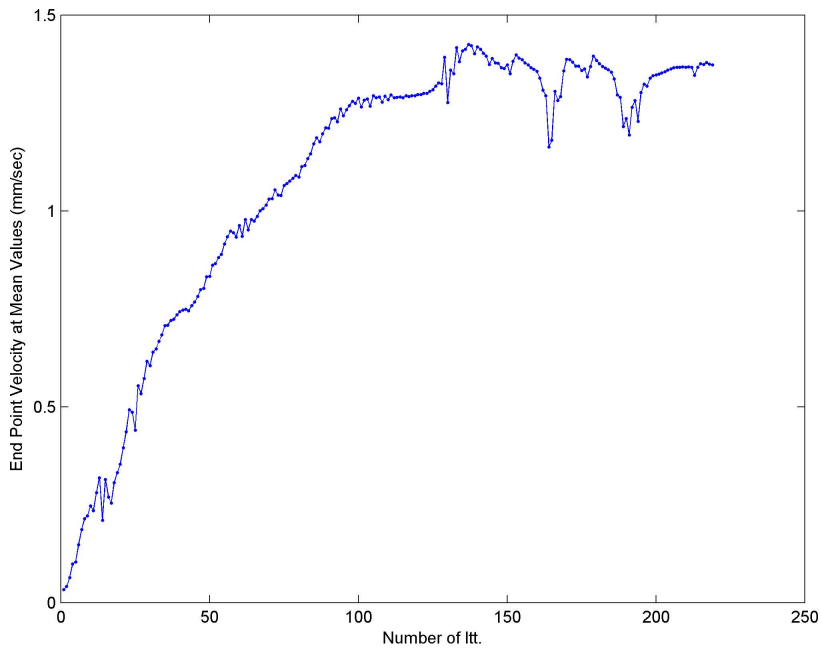
(a)

(b)

(c)

(d)

(e)

Figure 12: DTO designs with 50% volume fraction for :(a) Q4-FEM, (b) T3-FEM, (c) CS-FEM (*nSD=2*), (d) CS-FEM (*nSD=4*), and (e) CS-FEM (*nSD=8*).
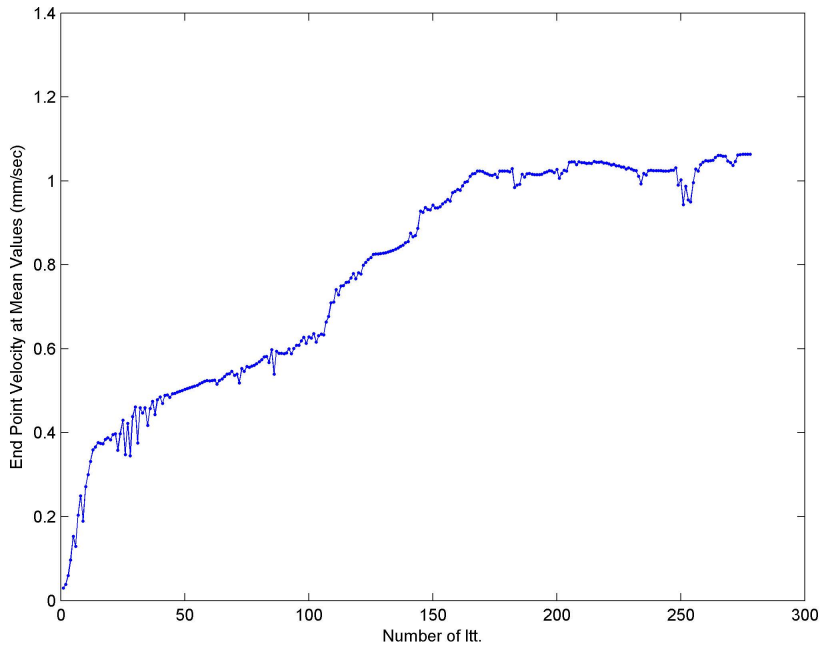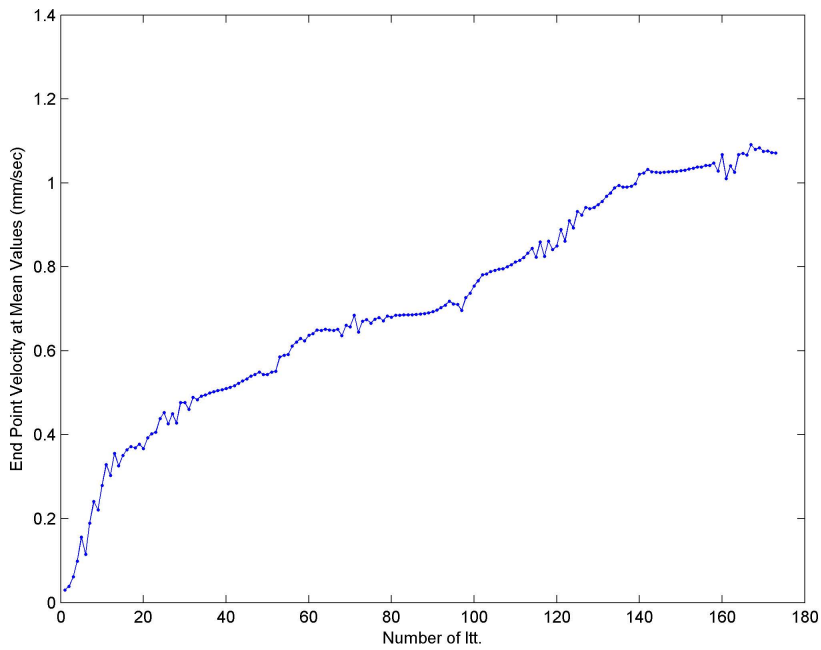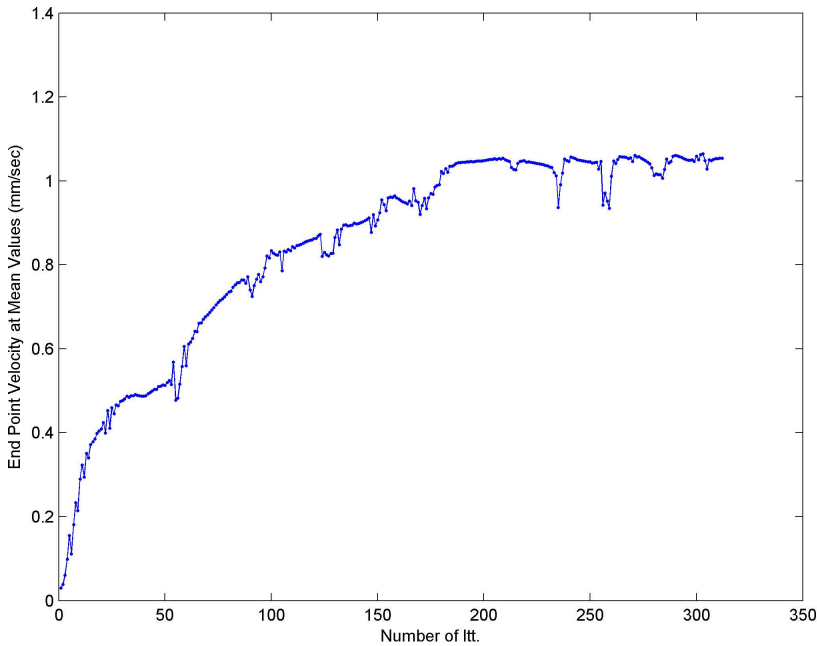
(a)
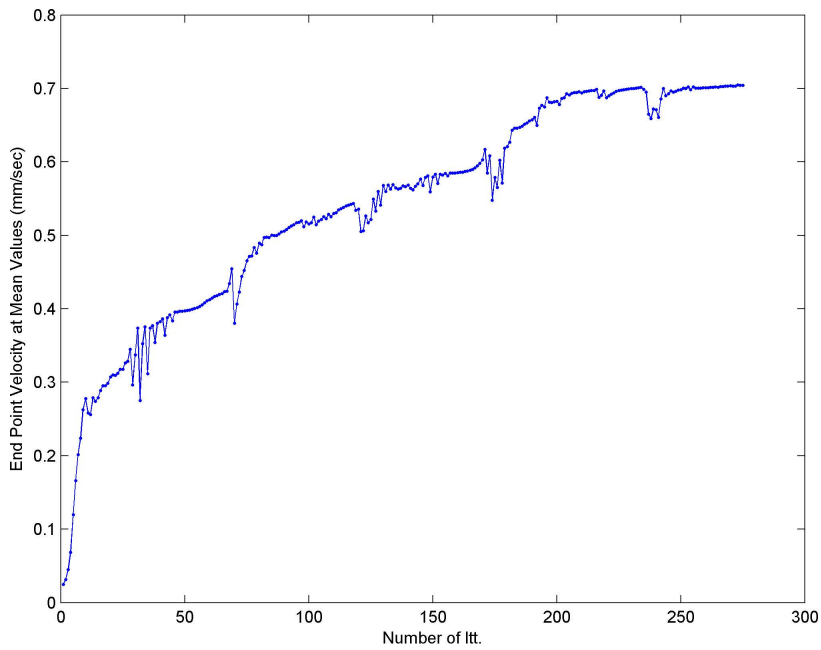
(b)

(c)

(d)

(e)

Figure 13: RBTO ($\beta_t = 3$) designs' velocity convergence rates (50% volume fraction) at the mean random values for: (a) Q4-FEM, (b) T3-FEM, (c) CS-FEM (*nSD=2*), (d) CS-FEM (*nSD=4*), and (e) CS-FEM (*nSD=8*).

increased (from 2 to 8), the optimized velocity approached the Q4-FEM results. This observation services, in a way, a validation of the CS-FEM for determining topology optimization designs when many smoothing domains are used.

From S-FEM theory, see Liu and Nguyen (2010), we know that the S-FEM model becomes stiffer with an increase of the smoothing domains. Therefore, by using fewer smoothing domains, we can obtain a softer CS-FEM model, and hence achieve more accurate solution-which is important for our RBTO problem.

Another important difference between the standard FEM and CS-FEM techniques for topology optimization evaluation is final design patterns obtained. As can be seen from optimization results, tables 2 and 3, optimal design configurations, figures 12 and 14, and even reanalysis results, table 5, unlike the Q4-FEM and T3-FEM, final topology optimization designs for the DTO and RBTO through the CS-FEM, have more distinguishable values and configurations. But the DTO and
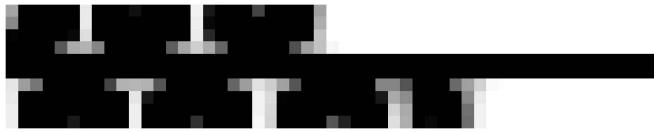
(a)

(b)

(c)

(d)

(e)

Figure 14: RBTO designs ($\beta_t = 3$) with 50% volume fraction for :(a) Q4-FEM, (b) T3-FEM, (c) CS-FEM (nSD=2), (d) CS-FEM (nSD=4), and (e) CS-FEM (nSD=8).

(a)

(b)

(c)

(d)

(e)

Figure 15: DTO reanalysis designs with 0.6 threshold factor for :(a) Q4-FEM, (b) T3-FEM, (c) CS-FEM (*nSD=2*), (d) CS-FEM (*nSD=4*), and (e) CS-FEM (*nSD=8*).

(a)

(b)

(c)

(d)

(e)

Figure 16: BBTO ($\beta_t = 3$) reanalysis designs with 0.6 threshold factor for :(a) Q4-FEM, (b) T3-FEM, (c) CS-FEM (*nSD=2*), (d) CS-FEM (*nSD=4*), and (e) CS-FEM (*nSD=8*).

Table 3: Comparisons of our RBTO ($\beta_t = 3$) designs with 50% volume fraction.

FEM method	Initial velocity at mean random values (mms^{-1})	Optimized velocity at mean random values (mms^{-1})	Number of iterations	Total CPU time (min)
Q4-FEM	0.0297	1.0619	278	60.5
T3-FEM	0.0249	0.7042	275	56.5
CS-FEM (*nSD=2*)	0.0329	1.3726	219	44.3
CS_FEM (*nSD=4*)	0.0304	1.0712	173	48.4
CS_FEM (*nSD=8*)	0.0299	1.064	312	114.3

Table 4: Comparison of our final reanalysis designs (Threshold factor: 0.6).

FEM method	DTO($\beta_t = 0$)		RBTO($\beta_t = 3$)	
	Optimum velocity (mms^{-1})	Volume ratio	Optimum mean velocity (mms^{-1})	Volume ratio
Q4-FEM	0.588	0.479	0.558	0.479
T3-FEM	0.4318	0.487	0.4265	0.483
CS-FEM (*nSD=2*)	0.4267	0.468	0.4205	0.475
CS-FEM (*nSD=4*)	0.6558	0.482	0.6136	0.491
CS-FEM (*nSD=8*)	0.585	0.477	0.5705	0.482

RBTO designs by the Q4-FEM technique almost have similar configurations and even the amounts of optimized velocities are very close. This shows that optimizations using the softer CS-FEM are preferable to those using the standard FEMs.

Finally, because a smoothed strain is used inside each smoothing domain in the CS-FEM, by increasing the number of smoothing domains the final topology optimized results will have fewer checkerboard or gray regions than even the designs obtained by standard FEMs, see Huang and Xie (2010). Indeed, as can be observed from the obtained results, after the reanalysis process the optimized velocity for CS-FEM (*nSD=2*) is less than the velocity from CS-FEM (*nSD=4*).

Table 5: Comparisons of our DTO and RBTO reanalysis designs in summary.

FEM method	DTO($\beta_t = 0$)		RBTO($\beta_t = 3$)	
	Optimum velocity (mms⁻¹)	Optimum configuration	Optimum mean velocity (mms⁻¹)	Optimum configuration
Q4-FEM	0.588		0.558	
T3-FEM	0.4318		0.4265	
CS-FEM (*nSD=2*)	0.4267		0.4205	
CS-FEM (*nSD=4*)	0.6558		0.6136	
CS-FEM (*nSD=8*)	0.585		0.5705	

In our study, because the final reanalysis optimal objective function (linear velocity) obtained through CS-FEM (*nSD=4*) has a higher value than the other designs (e.g., more than about 10% with respect to the Q4-FEM result), and because this method usually has a more reasonable accuracy respect to the other numerical methods (for this type of problem), see Liu, Dai and Nguyen (2007), we suggest that *nSD=4* leads to the optimal solution.

7　Conclusions

Piezoelectric microactuators are extensively being used in industrial and medical science technologies. However, to attain even higher operational and economic efficiency, the optimum design of these structures is required. It is essential to ensure reliability during optimization procedures; most are due to inherent variations incurred during the manufacturing processes of these systems.

The topology optimization of a prescribed linear piezoelectric micromotor needed to reach maximum velocity by satisfying the 50% volume (weight) fraction and 0.135% probability of failure has been evaluated in this research. This optimization was determined using a softer cell based smoothed FEM (as a branch of smoothed FEMs), and the results were then compared to standard FEMs. A comparison of the RBTO and DTO results shows that the RBTO results using the softer cell-based smoothed FEM, with *nSD=4*, is preferred.

The considered micromotor is currently being produced commercially, and we have shown here that it can substantially improve the efficiency of piezoelectric micromotors. However, it was also noted that smoothed-FEMs are usually more effective for nonlinear systems; hence, this type of optimization can be developed in as a future study.

References

Allen, M.; Raulli, M.; Maute, K.; Frangopol, D.M. (2004): Reliability-based analysis and design optimization of electrostatically actuated MEMS. *Comput. Struct.*, Vol.82, pp.1007-1020.

Allik, H.; Hughes, T. J. R. (1970): Finite element method for piezo-electric vibration, *Int. J. Numer. Meth. Eng.*, Vol. 2, pp. 151-157.

Bae, K.; Wang, S.; Choi, K.K. (2002): Reliability-based topology optimization. *In: AIAA 2002-5542, 9th AIAA/ISSMO.*

Begg, D.W.; Liu. X. (2000): On simultaneous optimization of smart structures-Part II: Algorithms and examples. *Comput. Methods Appl. M.*, Vol. 184, pp. 25-37.

Bendsoe, M.P. (1989): Optimal shape design as a material distribution problem. *Struct. Optimization.*, Vol. 1, pp.193-202.

Bendsoe, M.P.; Kikuchi, N. (1988): Generating optimal topologies in structural design using a homogenization method. *Comput. Methods Appl. M.*, Vol.71, pp.197-224.

Bendsoe, M.P.; Sigmund, O. (1999): Material interpolations in topology optimization. *Arch. Appl. Mech.*, Vol. 69, pp.635–654.

Bendsoe, M.P.; Sigmund, O. (2003): *Topology Optimization: Theory, Methods and Applications*. Springer, Berlin.

Benjeddou, A. (2000): Advances in piezoelectric finite element modeling of adaptive structural elements: a survey. *Comput. Struct.*, Vol.76, pp. 347-363.

Bordas, S.P.A.; Rabczuk. T.; Hung, N.X.; Nguyen, V.P; Natarajan, S.; Bog, T.; Quan, D.M.; Hiep, N.V. (2010): Strain smoothing in FEM and XFEM. *Comput. Struct.*, Vol.88, pp.1419-1443.

Buslenko, N. P.; Golenko, F. I.; Shreider, Y. A.; Sobol, I. M.; Sragowich, V. G. (1964): *The Monte Carlo Method,* Press, New York.

Carbonari, R.C.; Nader, G.;Silva, E.C.N. (2006): Experimental and numerical characterization of piezoelectric mechanisms designed using topology optimization. *Int. ABCM symposium series in Mechatronics* ,Vol.2, pp.425-432.

Carbonari, R.C.; Silva, E.C.N.; Nishiwaki, S. (2005): Design of piezoelectric multi-actuated microtools using topology optimization. *Smart Mater. Struct.*, Vol.14 , pp. 1431-1447.

Chen, J.S.; Wu, C.T.; Yoon, S. Y. (2001): A stabilized conforming nodal integration for Galerkin mesh-free methods. *Int. J. Numer. Meth. Eng.*, Vol.50, pp.435-466.

Choi, K.K.; Kim, N.H. (2005): *Structural Sensitivity Analysis and Optimization*. Springer Science and Business Media, Inc., New York.

Dai, K.Y.; Liu, G.R.; Nguyen, T.T. (2007): An n-sided polygonal smoothed finite element method (nSFEM), for solid mechanics. *Finite Elem. Anal. Des.*, Vol.43, pp. 847-860.

Ditlevsen, O.; Madsen, H. (1996): *Structural Reliability Methods*. New York: John Wiley & Sons.

Donoso, A.; Sigmund, O. (2009): Optimization of piezoelectric bimorph actuators with active damping for static and dynamic loads. *Struct. Multidiscip. O.*, Vol.38,pp.171-183.

Du, J.; Olhoff, N. (2007): Topological design of freely vibrating continuum structures for maximum values of simple and multiple eigenfrequencies and frequency gaps. *Struct. Multidiscip. O.*, Vol. 34, pp.91-110.

Frangopol, D.M. (1995): Reliability-based optimum structural design. *Probabilistic Structural Mechanics Handbook*. New York: Chapman & Hall, pp. 352–387.

Frecker, M.I. (2003): Recent advances in optimization of smart structures and actuators. *J. Intel. Mat. Syst. Str.*, Vol. 14, pp.207-216.

Friend, J.; Umeshima, A.; Ishii, T.; Nakamura, K.; Ueha, S. (2004): A piezoelectric linear actuator formed from a multitude of bimorphs. *Sensor. Actuat. A-Phys.*, Vol. 109, pp. 242-251.

Hasofer, A.M.; Lind, N.C. (1974): An exact and invariant first order reliability format. *J. Eng. Mech-ASCE*, Vol.100, pp.111-121.

Hohenbichler, M.; Rackwitz, R. (1981): Normal dependent vectors in structural reliability. *J. Eng. Mech. Div. ASCE*, Vol.107 (6), pp.1227-1238.

Huang, X.; Xie, Y.M. (2010): *Evolutionary Topology Optimization of Continuum Structures Methods and Applications*, John Wiley and Sons Ltd.

Irschik, H. (2002): A review on static and dynamic shape control of structures by piezoelectric actuation. *Eng. Struct.,* Vol.24 (1), pp.5-11.

Jensen, J. S. (2009): *A Note on Sensitivity Analysis of Linear Dynamic Systems with Harmonic Excitation, Report*. Department of Mechanical Engineering, Tech-

nical University of Denmark.

Jae-Ohk, L.; Young-Soon, Y.; Wom-Sun, R. (2002): A comparative study on reliability and target-performance-based probabilistic structural design optimization. *Comput. Struct.* , Vol. 80, pp. 257-269.

Kang, Zh.; Wang, X. (2010): Topology optimization of bending actuators with multilayer piezoelectric Material. *Smart Mater. Struct.*, Vol.19, 075018(11p).

Kharmanda, G.; Olhoff, N.; El-Hami, A. (2004): Optimum values of structural safety factors for a predefined reliability level with extension to multiple limit states, *Struct. Multidiscip. O.*, Vol. 27, pp 421-434.

Kharmanda, G.; Olhoff, N.; Mohamed, A.; Lemaire, M. (2004): Reliability-based topology optimization, *Struct. Multidiscip. O.,* Vol.26, pp.295-307.

Kim, J.E.; Kim, D.S.; Ma, P.S.; Kim, Y.Y. (2010): Multi-physics interpolation for the topology optimization of piezoelectric systems. *Comput. Method. Appl. M.*, Vol.199, pp.3153-3168.

Kim, C.; Wang, S.; Bae, K.; Moon, H. (2006): Reliability-based topology optimization with uncertainties. *KSME. Int. J.*, Vol.20 (4), pp.494-504.

Kim, C.; Wang, S.; Hwang, I.; Lee, J. (2005): Parallel computed reliability-Based topology optimization using response surface method. *6th World Congresses of Structural and Multidisciplinary Optimization.*

Kogl, M.; Silva, E.C.N. (2005): Topology optimization of smart structures: design of piezoelectric plate and shell actuators. *Smart Mater. Struct.* , Vol.14 , pp. 387–399.

Liu, G.R. (2009): *Meshfree Methods – Moving beyond the finite element method.* 2nd Edn., CRC Press.

Liu, G.R.; Dai, K.Y.; Lim, K.M.; Gu, Y.T. (2003): A radial point interpolation method for simulation of two- dimensional piezoelectric structures. *Smart Mater. Struct.*, Vol. 12, pp. 171-180.

Liu, G.R.; Dai, K.Y.; Nguyen, T.T. (2007): A smoothed finite element method for mechanics problems. *Comput. Mech.*, Vol.39, pp. 859-877.

Liu, G.R.; Nguyen, T. T. (2010): *Smoothed Finite Element Methods*, CRC press, Taylor and Francis group.

Liu, G.R.; Nguyen, T.T.; Dai, K. Y.; Lam, K.Y. (2007): Theoretical aspects of the smoothed finite element method (SFEM). *Int. J. Numer. Meth. Eng.*, Vo.71, pp.902-930.

Liu, G.R.; Nguyen, T. T. ; Lam, K.Y. (2009): An edge-based smoothed finite element method (ES-FEM) for static, free and force vibration analyses of solids .*J.*

*Sound Vib.,*Vol. 320, pp. 1100-1130.

Liu, G.R.; Nguyen-X.H.; Nguyen, T.T. (2010): A theoretical study on the smoothed FEM (S-FEM) models: Properties, accuracy and convergence rates, *J. Numer. Meth. Eng.*, Vol.84 (10), pp.1222-1256.

Long, C. S.; Loveday, P. W.; Groenwold, A. A. (2006): Planar four node piezo-electric with drilling degrees of freedom. *Int. J. Numer. Meth. Eng.,* Vol. 65, pp.1802-1830.

Luo, Y.; Kang, Z.; Luo, Z.; Li, A. (2009): Continuum topology optimization with non-probabilistic reliability constraints based on multi-ellipsoid convex model. *Struct. Multidiscip. O.*, Vol.39, pp.297-310.

Madsen, H.O.; Krenk, S.; Lind, N.C. (1986): *Methods of Structural Safety*. Prentice-Hall, Englewood Cliffs, NJ.

Moskalik, A.J.; Brei, D. (1999): Force-deflection behavior of piezoelectric C-block actuator arrays .*Smart Mater. Struct.* , Vol.8, pp. 531-543.

Nguyen, X.H.; Liu, G.R.; Nguyen, T.T.; Nguyen, C.T. (2009): An edge-based smoothed finite element method for analysis of two-dimensional piezoelectric struc-tures. *Smart Mater. Struct.*, Vol.18 (6), 065015(12pp).

Nocedal, J. ; Wrigh, S.J. (2006): *Numerical optimization*, Second edition ,Springer.

Ohs, R. R.; Aluru, N. R. (2001): Meshless analysis of piezoelectric devices. *Comput. Mech.*, Vol.27, pp. 23-36.

Rackwits, R.; Fiessler, B. (1978): Structural reliability under combined random load sequences. *Comput. Struct.*, Vol.9, pp.489-494.

Raulli, M.; Maute, K. (2009): Reliability based design optimization of MEMS Considering Pull-in. *J. Mech. Design-T ASME*, Vol.131 (6), 061014(10 pages).

Rozvany, G.; Zhou, M.; Birker, T. (1992): Generalized shape optimization with-out homogenization. *Struct. Optimization*, Vol. 4, pp.250-254.

Silva, E.C.N. (2003): Topology optimization applied to the design of linear piezo-electric motors, *Smart Mater. Struct.*, Vol. 14, pp.309-322.

Silva, R.C.N.; Kikuchi, N. (1999): Design of piezocomposite materials and piezo-electric transducers using topology optimization- part III. *Arch. Comput. Method E.,* Vol. 6, pp.305-329.

Spillers, W.R.; MacBain, K.M. (2009): *Structural optimization* , Springer science + Business media.

Stark, B. (1999): *MEMS Reliability Assurance Guidelines for Space Applications*. Jet Propulsion Laboratory, Technical Report.

Svanberg, K. (1987): Method of moving asymptotes—a new method for structural

optimization, *Int. J. Numer. Meth. Eng.*, Vol.24, pp.359-373.

Sze, K. Y.; Yang, X. M.; Yao, L. Q. (2004): Stabilized plane and axisymmetric piezoelectric finite element models. *Finite Elem. Anal. Des.* Vol. 40, pp. 1105-1122.

Tbata, O.; Tsuchiya, T. (2007): *Advanced Micro&Nanosystems. Reliability of MEMS*. Wiley-VCH Verlag Gmbh&Co.KGaA, Vol.6.

Ueha, S.; Tomikawa, Y. (1993): *Ultrasonic Motors-Theory and Applications*. Monographs in Electrical and Electronic Engineering, Vol.29, Clarendon Press, Oxford.

Wang, Q.M. ; Zhang, Q. ; Xu, B. ; Liu, R. ; Cross, L.E. (1999): Nonlinear piezo-electric behavior of ceramic bending mode actuators under strong electric fields. *J. Appl. Phys.*, Vol. 86(6), pp.3352-3360.

Wu.Y.T. (1994): Computational methods for efficient structural reliability and reliability sensitivity analysis . *AIAA . J.*, Vol. 32(8), pp.1717-1723.

Yang, J. (2006): *Analysis of Piezoelectric Devices*, World Scientific Publishing Co. Pte. Ltd.

Youn, B.D.; Choi, K.K.; Park, Y.H. (2003): Hybrid analysis method for reliability-based design optimization. *J. Mech. Design-T ASME*, vol. 125, pp. 221-232.